Supporting Information

for

Selenomelanin: An Abiotic Selenium Analogue of Pheomelanin

Wei Cao, Naneki C. McCallum, Qing Zhe Ni, Weiyao Li, Hannah Boyce, Haochuan Mao, Xuhao Zhou, Hao Sun, Matthew P. Thompson, Claudia Battistella, Michael R. Wasielewski, Ali Dhinojwala, Matthew D. Shawkey,* Michael D. Burkart,* Zheng Wang,* Nathan C. Gianneschi*

Correspondence to: matthew.shawkey@ugent.be, mburkart@ucsd.edu, zheng.wang@nrl.navy.mil, or nathan.gianneschi@northwestern.edu.

This PDF file includes:

Supplementary Information Text

Materials and Methods

Materials

L-3,4-dihydroxyphenylalanine (L-DOPA), tris(2-carboxyethyl) phosphine hydrochloride (TCEP·HCl), cysteine and potassium permanganate ($KMnO_4$) were purchased from Fisher Scientific. Selenocystine was purchased from Chempep Inc. Propidium iodide (PI), Wheat Germ Agglutinin (WGA) conjugated to Alexa Fluor 633 or 488, Hoechst 33342, DNase-free RNase, and 2' ,7' -dichlorofluorescein diacetate (DCFDA) were purchased from ThermoFisher Scientific. SingleShot™ SYBR® Green Kit for Cell Lysis and RT-qPCR was purchased from Bio-Rad. All reagents and materials were used as received unless otherwise stated.

Instrumentation

Nanoparticle characterization:

Dynamic Light Scattering (DLS) measurements were performed on a DynaPro Nanostar (Wyatt Technology Corp) at room temperature in ultrapure water at around 0.05 mg mL^{-1}. Zeta potential was measured on a Malvern Zetasizer in ultrapure water at room temperature. UV-Vis spectra were collected on a Cary Series 100 UV-Vis spectrophotometer. Circular dichroism spectra were measured on a Circular Dichroism Spec J-815 in Keck Biophysics Facility (KeckBio) at Northwestern University. FTIR spectra were collected on a Nexus 870 spectrometer (Thermo Nicolet) in NU Atomic and Nanoscale Characterization Experimental Center (NUANCE) at Northwestern University. ICP-OES (Inductively coupled plasma - optical emission spectrometry) was performed on a computer-controlled (QTEGRA software) Thermo iCap7600 ICP-OES (Thermo Fisher Scientific, Waltham, MA, USA) operating in axial view and equipped with a CETAC 520 autosampler (Omaha, NE, USA) at Northwestern University. For scanning electron microscope (SEM) images, particles were drop-casted onto aluminum SEM stubs and dried overnight. They were plasma coated with 10 nm osmium and then imaged immediately using a Hitachi SU8030 cFEG SEM at 10.0 kV and an emission current of 15 mA. For scanning transmission electron microscopy (STEM) images, particles were drop-casted onto 400 mesh formvar/carbon grids (Ted Pella), which were first surface plasma treated using a PELCO easiGlow glow discharge cleaning system. Images were obtained on a Hitachi HD2300 cFEG STEM with a bright field detector at 200 kV and an emission current of 57 μA.

For cell experiments:

CellTiter-Blue® fluorescence measurements were recorded using a Perkin Elmer EnSpire ultimode Plate Reader. Confocal laser scanning microscopy (CLSM) images were obtained on a Leica SP5 laser scanning confocal microscope in the Biological Imaging Facility (BIF) at Northwestern University. Cell cycle tests were performed on an E.A1 LSR Fortessa 2 cell analyzer in the Flow Cytometry Core at Northwestern University. Cell viability based on flow cytometry using PI was performed on a Beckman Coulter CytoFLEX Flow Cytometer in the Gianneschi lab.

Methods

Preparation of synthetic selenomelanin.

We synthesized selenomelanin nanoparticles (SeNPs) by oxidative copolymerization of selenocysteine and L-3,4-dihydroxyphenylalanine (L-DOPA) using $KMnO_4$ in ultrapure water (pH=7) at room temperature. The reaction is a templated polymerization reaction with L-DOPA eumelanin nanoparticle as the seeds. First, 120 mg (0.6 mmol) of L-DOPA was dissolved in 100 mL water and then mixed with 1.8 mL $KMnO_4$ (31.6 mg mL^{-1}, 0.2 M) in a 250 mL round-bottom flask for 30 minutes to form eumelanin seeds. Next, a selenocysteine solution was added to the reaction flask in one portion (selenocysteine is not stable and therefore was formed *in situ* by adding 86 mg TCEP·HCl (0.3 mmol) to a degassed solution of selenocystine (122 mg, 0.3 mmol), and the pH was adjusted to 7 using 1 M NaOH solution). After overnight reaction, the product was collected by centrifugation at 4 ℃ (11500 rpm for 15 min) and purified by washing with 3 mL of 1 M HCl solution to exchange the Mn^{2+} ions and subsequent washing with ultrapure water three times. Finally, the mass concentration of the final nanoparticle solution was determined by lyophilizing a small aliquot solution overnight and weighing with an analytical balance.

Selenomelanin can also be generated without first forming pure L-DOPA eumelanin seeds. This approach yields irregular morphologies rather than SeNPs (Supplementary Information, **Fig. S1B**).

Preparation of synthetic pheomelanin.

We performed pheomelanin synthesis as reported by Lee *et al.*[1] Briefly, 140 mg of L-DOPA (0.7 mmol) and 171.2 mg (0.7 mmol) of L-cysteine were dissolved in 100 mL of water under sonication. Then, 720 μL of a 0.2 M $KMnO_4$ solution (31.6 mg mL^{-1}, 0.2 M) was quickly added. The reaction was stirred for 24 h at room temperature. The resulting NPs were purified by centrifugation at 11000 rpm for 10 min at room temperature, followed by washing in 3 mL of a 1 M HCl solution to exchange the Mn^{2+} ions, and triple washed with ultrapure water.

Preparation of synthetic L-DOPA nanoparticles.

As reported by Lee *et al,*[1] 280 mg of L-DOPA (1.4 mmol) was dissolved in 100 mL of ultrapure water, 1.44 mL of a $KMnO_4$ solution (31.6 mg mL^{-1}, 0.2 M) was quickly injected into the solution, and the reaction was stirred vigorously at room temperature for 24 h. The resulting NPs were purified by centrifugation at 11000 rpm for 10 min, followed by washing in 3 mL of a 1 M HCl solution to exchange the Mn^{2+} ions, and three more cycles of washing and centrifugation with ultrapure water.

Pheomelanin extraction from the covert feathers of a Rhode Island red rooster.

We isolated intact melanosomes following the enzymatic (Proteinase-K based) extraction method of Liu et al (2004).[2] Compared to other, harsher methods traditionally employed in melanin extraction (e.g. acid-base extraction), this method retains the integrity of the chemical composition of melanin. Briefly, 10 g of feathers were initially washed by a series of organic solvents, including acetone, dichloromethane, ether, and ultrapure water and cut into 2 mm pieces. Then the feather pieces were treated with DTT, Proteinase-K and papain. After another round of treatment with Proteinase-K, Triton X-100 and Proteinase-K, the pheomelanin was obtained as a red to brown suspension in water and lyophilized overnight for ssNMR. The total amount of pheomelanin obtained was 48 mg.

Solid State NMR.

Approximately 30 mg of lyophilized sample was packed into a 3.2 mm Bruker rotor. Each 1D ^{13}C cross polarization (CP) was acquired using 36 k scans and a recycle delay of 3 s on a 750 MHz Bruker spectrometer. The CP contact time was optimized to 2 ms and the ^{1}H decoupling was 83 kHz. The spinning speed was 13.5 kHz. All ^{13}C NMR spectra were recorded with complete proton decoupling. FID files were processed using MestRenova 7 software (Mestrelab Research).

Transmission Electron Microscopy and Scanning Transmission Electron Microscopy.

TEM of particles: Transmission electron microscopy (TEM) micrographs were obtained on a Hitachi 7700 TEM. TEM samples were prepared by drop casting 10 μL of sample solution in water onto the copper grid (lacey carbon, 300 mesh, from Ted Pella) without further staining.

STEM of cells: NHEK cells were seeded on 13 mm Thermanox™ coverslips and fixed in 0.1 M sodium phosphate or PIPES buffer with 2.5% glutaraldehyde and 2% paraformaldehyde. The cells were microwaved using a Pelco Biowave and post-fixed with 1% OsO_4 in imidazole followed by 1% uranyl acetate. The cells were dehydrated with a series of ethanol and acetone treatments and then permeated with EMBed812 resin in BEEM® capsules. The resin was polymerized by heating to 60 °C for 48 hours. Ultramicrotomy was performed using a Leica EM UC7 Ultramicrotome and the cells sectioned to 80 nm thick. Sections were mounted onto 1-2 mm slotted or 300 mesh copper grids with carbon support and stained for 20 minutes with 2% uranyl acetate. Images were obtained on a Hitachi HD2300 cFEG STEM with an HAADF detector at 80 kV and an emission current of 57 μA. The images were contrast-inverted to reflect the appearance of standard bright field TEM images.

NHEK *in vitro* Cell Culture Studies.

Primary neonatal epidermal keratinocyte (NHEK) cells were isolated from freshly excised neonatal foreskins and gifted by the Perez-White lab at Northwestern Feinberg School of Medicine. M154 medium supplemented with human keratinocyte growth supplement (HKGS), 10 μg mL^{-1} gentamicin, 0.25 μg mL^{-1} amphotericin B, and 0.07 mM $CaCl_2$ was used to incubate the cells. Cells were maintained at 37 °C and 5% CO_2 with a relative humidity of 95%.

X-ray related experiments were performed in a Radsource-2000 X-ray irradiator (Model: RS200, Serial: 3239) operated at 160 kV voltage and 25 mA. The gray (Gy) unit is defined as the absorption of one joule of radiation energy per kilogram of matter. 1 Gy= 1 J kg^{-1}. The X-ray dose rate was 4.446 Gy min^{-1} at shelf level 5. A vinyl coated lead sheet (5.1×30.5 cm) with 2.2 mm thickness was purchased from Fisher Scientific to selectively shield X-ray irradiation.

For biocompatibility assays, NHEK cells were plated in 48-well plates at a density of 5 k per well and then left to seed for 24 h. Subsequently, the cells were treated with NPs for the desired time followed by washing 3 times with PBS. After the incubation period, CellTiter-Blue® at 10% (v/v) in complete media was added to each well and incubated for 2 h to allow the live cells to convert resazurin to fluorescent resorufin. The fluorescent signal was then analyzed with excitation wavelength at 560 nm and emission wavelength at 600 nm by a plate reader. Three replicates were performed for each independent sample. 10% DMSO was used as a positive control, and untreated cells in complete medium as a negative control. Viability is reported as a percentage of untreated cells, averaged over three biological repeats.

NHEK cells were plated in 4-well, glass bottom dishes at 5k cells per well and seeded for 24 h before treatment with NP suspensions for another 24 h. The cells were stained with 5 μg mL^{-1} of WGA conjugated to Alexa Fluor 633 in DPBS for 10 minutes at room temperature, washed with PBS, and returned to complete growth medium. Before imaging, 1 drop of Hoechst 33342 dye was added to stain the nuclei. WGA 633 scan excitation wavelength: 633 nm. Detection Wavelength: 650-690 nm. Hoechst scan excitation wavelength: 405 nm. Detection Wavelength: 420 nm to 480 nm.

Cell cycle studies were performed according to a protocol by Abcam.[3] NHEK cells were plated at a density of 50k cells per well in 12-well plates. After incubating for 24 h, nanoparticles of varying concentrations were added to each well for 24 h. Then X-ray radiation was applied at the dose rate of 4.4 Gy min^{-1}. The cells were incubated for the desired times before assaying experiments were performed.

ROS scavenging experiments on NHEK cells were performed by first incubating with NPs (0.004 mg mL^{-1}) for 24 h. The cells were then treated with 0.8 μM of the ROS probe DCFDA, incubated at 37 °C for 20 min. Next, the loading buffer was removed, and cells were returned to the growth medium. Then, the cells were irradiated with 6 Gy X-ray. A drop of Hoechst 33342 dye was added to 0.5 mL media for the nucleus staining before imaging by CLSM. Live-cell imaging was performed on a Leica SP5 confocal microscope with the smart gain at 70% and laser power at 12% for the entire series. ROS probe scan excitation wavelength: 486 nm. Detection Wavelength: 510-550 nm. Hoechst scan excitation wavelength: 405 nm. Detection Wavelength: 420 nm to 480 nm.

Radical scavenging DPPH assay.

DPPH (2,2-Diphenyl-1-(2,4,6-trinitrophenyl) hydrazyl) radical scavenging activity of SeNP was measured according to the procedure by Lee J. K.[4, 5] Briefly, 100 μL of a 0.6 mg/mL suspension of SeNP in ultrapure water was mixed with 1.8 mL of a 0.2 mM DPPH solution in 95% ethanol. The scavenging activity was evaluated by monitoring the absorbance decrease at 516 nm over 20 min. DPPH radical scavenging activity was calculated as

$I = [1 - (Ai - Aj)/Ac] * 100\%$

where *Ac* is the absorbance of DPPH solution without SeNP, *Ai* is the absorbance of SeNP mixed with the DPPH solution, and *Aj* is the absorbance of SeNP without DPPH.

Vibrio natriegens biosynthesis of selenomelanin materials.

Melanin producing *V. natriegens* were constructed and cultured according to a published procedure.[6] Marine bacterium *V. natriegens* was engineered to express a heterologous tyrosinase gene and cultured for 24 h in medium containing (1) 2 mM L-DOPA, (2) 2 mM L-DOPA plus 2 mM cysteine, or (3) 2 mM L-DOPA plus 2 mM selenocystine. Melanized bacteria were then incubated with 4 M guanidinium thiocyanate solution at room temperature for 30 min. Cells were washed with deionized water once and hydrolyzed by boiling in 6 M HCl for 30 min. The resulting black material ("melanin ghosts") were washed with deionized water multiple times until the pH increased to 6. Melanin nanoparticles were collected from the culture medium supernatant with a 200 nm filter.

Extinction coefficient measurement

The extinction coefficient of NPs was determined by measuring the UV-Vis spectra of the melanin solutions at different concentrations. Five different concentrations were used for extinction coefficient measurement.

X-ray Photoelectron Spectroscopy

X-ray photoelectron spectroscopy (XPS) samples were drop-casted onto a silicon substrate, and spectra were collected on a Thermo Scientific ESCALAB 250Xi.

Circular dichroism measurement

CD spectra were measured from 190 to 300 nm with a slit width of 1 nm, scanning at 1 nm intervals with a 1s integration time. Measurements were taken 3 times at 25°C under a nitrogen atmosphere and then averaged to give the spectra.

Electron Paramagnetic Resonance Spectroscopy

Continuous wave EPR spectra were obtained at X-band (9.5 GHz) fields using a Bruker Elexsys E680 spectrometer equipped with a 4122SHQE resonator. Scans were performed with a magnetic field modulation amplitude of 2 G and non-saturating microwave power of 1.544 mW. The results are the average of 32 scans. Samples were contained in quartz tubes with I.D. 1.50 mm and O.D. 1.80 mm. For quantification, 4-amino-TEMPO was dissolved in ultrapure water as a spin standard. EPR spectra were taken of the standard solutions under identical conditions. The EPR spectra were double integrated and then the double integration areas were plotted against the spin concentration. The double integration of the SeNP at 5.4 mg mL^{-1} is 17.3. According to the calibration curve in **Fig. S3.**, the radical content is 1.12×10^{18} per gram, which is similar to the polydopamine and poly(L-DOPA) samples reported previously by Dadachova et al.[7]

ICP-OES detection of S and Se

PNP and SeNP samples were digested in concentrated trace nitric acid (>69%, Thermo Fisher Scientific, Waltham, MA, USA) at 65 °C for at least 3 hours. Ultrapure H_2O (18.2 MΩ·cm) was added to produce a final solution of 5.0% nitric acid (v/v) in a total sample volume of 6 mL. Quantitative standards consisting of 1000, 500, 250, 125, 62.5, and 31.25 ng g^{-1} of S and Se were prepared using a 1000 μg mL^{-1} S standard and a 100 μg mL^{-1} Se standard (Inorganic Ventures, Christiansburg, VA, USA) in 5.0% nitric acid (v/v) in a total sample volume of 5 mL. Each sample was acquired using a 5 second visible exposure time and 15 second UV exposure time, running 3 replicates. The spectral lines selected for analysis were: S (180.731, 182.034 nm) and Se (196.090, 203.985 nm).

Refractive index measurement

Solutions were prepared at a concentrations of 0.05 mg mL^{-1}, 0.1 mg mL^{-1}, 0.2 mg mL^{-1}, 0.3 mg mL^{-1}, 0.4 mg mL^{-1}, or 0.5 mg mL^{-1}. The real part of the RI of the solution (n_{eff}) was measured using a digital refractometer J157 (Rudolph Research Analytical, 589 nm), which was first calibrated using ultrapure water (n_w =1.33296) and ethanol (std n =1.36162). Each sample was measured three times and averaged over 20 scans for each step. Both calibration and measurements were performed at 25 °C.

Using the Drude model, the effective RI of the solution is given by the following equation:

$$n_{eff}^2 = V_m n_m^2 + (1 - V_m)\, n_w^2$$

Where V_m and n_m are the volume fraction and real part of the RI of particles, respectively; and n_w is the real part of the RI of water. We converted mass concentration into the volume fraction using the reported density of melanin, 1.3 g cm^{-3}.
n_m is determined by extrapolation of linear fitting of the data points (n_{eff}^2 versus V_m) at V_m=1.

RT-PCR for expression of the CDKN1a gene

Cells were lysed 3 h post-irradiation. Cell lysis, reverse transcription, and qPCR reactions were performed as per the instructions of the Single Shot SYBR Green kit from BioRad. Briefly, cells were washed with 3× DPBS (Gibco) followed by a 10 min incubation with the cell lysis mastermix consisting of 48 μL cell lysis buffer, 1 μL Proteinase K Solution, and 1 μL DNase Solution per well, prepared in advance on ice. Cell lysate was transferred to a 96 well PCR plate and incubated at 37 °C for 5 minutes followed by 5 minutes at 75 °C on a thermal cycler. Reverse transcription reactions were prepared on ice and included 4 μL iScript Advanced Reaction Mix, 1 μL iScript Advanced Reverse Transcriptase, 9 μL cell lysate, and 6 μL Nuclease-Free Water per well. Complete reaction mixes were incubated in a thermal cycler for 30 minutes at 42 °C followed by inactivation for 5 minutes at 85 °C. For the qPCR reaction 1.2 μL SsoAdvanced Universal SYBR Green Supermix and 1.2 μL cDNA diluted 10 times with Nuclease-Free Water were added to a 384 PCR plate using a TTP Labtech mosquito, and 60 nL each of the forward and reverse primers were added to the appropriate wells using a Labcyte Echo 550. The PCR plate was centrifuged and loaded into a BioRad CFX384 instrument and cycled through a 30 second activation at 98 °C followed by amplification using a 15 second denaturation step at 95 °C and 30 second annealing/extension step with a plate read at 60 °C for 40 cycles. Primer efficiency was validated with untreated cell lysates prior to test samples, and non-template controls and non-reverse transcriptase controls were also included for every primer pair. After completion of 40 cycles, samples were allowed to anneal at 50 °C for 1 minute, and melt curves were obtained by performing a 5 second incubation at 0.5 °C intervals from 65 °C to 98 °C. Data analysis was performed with CFX Manager software with no nanoparticles and 0 Gy radiation samples as controls.

<u>Cell cycle studies</u>
In a typical data analysis, forward and side scatter were plotted to identify the cells. Gating was used to eliminate the clumps and doublet cells. NHEK cells treated with no NP and no X-ray are shown as examples of the data analysis (**Fig. S17.**). Cell cycle data was analyzed using FlowJo v10.6.0 software. All data points shown are the average of at least three independent experiments. Student's two-tailed t-tests were used for the comparison of means of at least three independent experiments, and $P<0.01$ was considered statistically significant.

<u>Cell cycle changes over time after 6 Gy X-ray irradiation</u>
NHEK cells were treated with 6 Gy X-ray radiation and then incubated at 37 ⍰C with 5% CO_2 for varying periods of time. The cells were then harvested, fixed, and stained with PI for flow cytometry. Error bars represent the standard deviation of three independent experiments (**Fig. S18.**).

<u>Cell morphologies after 6 Gy X-ray irradiation</u>
To observe the morphology of cells after ionizing radiation, cells were irradiated using a Rad Source RS-2000 X-ray irradiator at a dose rate of 4.4 Gy min^{-1}. The cells were then incubated at 37 °C supplemented with 5% CO_2 for 24 h, fixed with 4% paraformaldehyde for 10 minutes, and stained with DAPI (10 min) and WGA conjugated to Alexa Fluor 488. Samples were then washed with DPBS three times and stored under DPBS in 4 °C fridge before imaging by CLSM (**Fig. S19.**). WGA 488 scan excitation wavelength: 486 nm. Detection Wavelength: 510-550 nm. Hoechst scan excitation wavelength: 405 nm. Detection Wavelength: 420 nm to 480 nm

<u>X-ray colorimetry film experiment</u>
We used dosimetry X-ray film and irradiated using 0-6 Gy. The X-ray dosage was found to be proportional to the absorbance of the film at λ_{max} 635 nm (R^2=0.98), validating that the film could be used to detect different X-ray dosages. Then, X-rays were impinged through a nanoparticle suspension (2 mL, 1 mg mL^{-1}) onto the film.

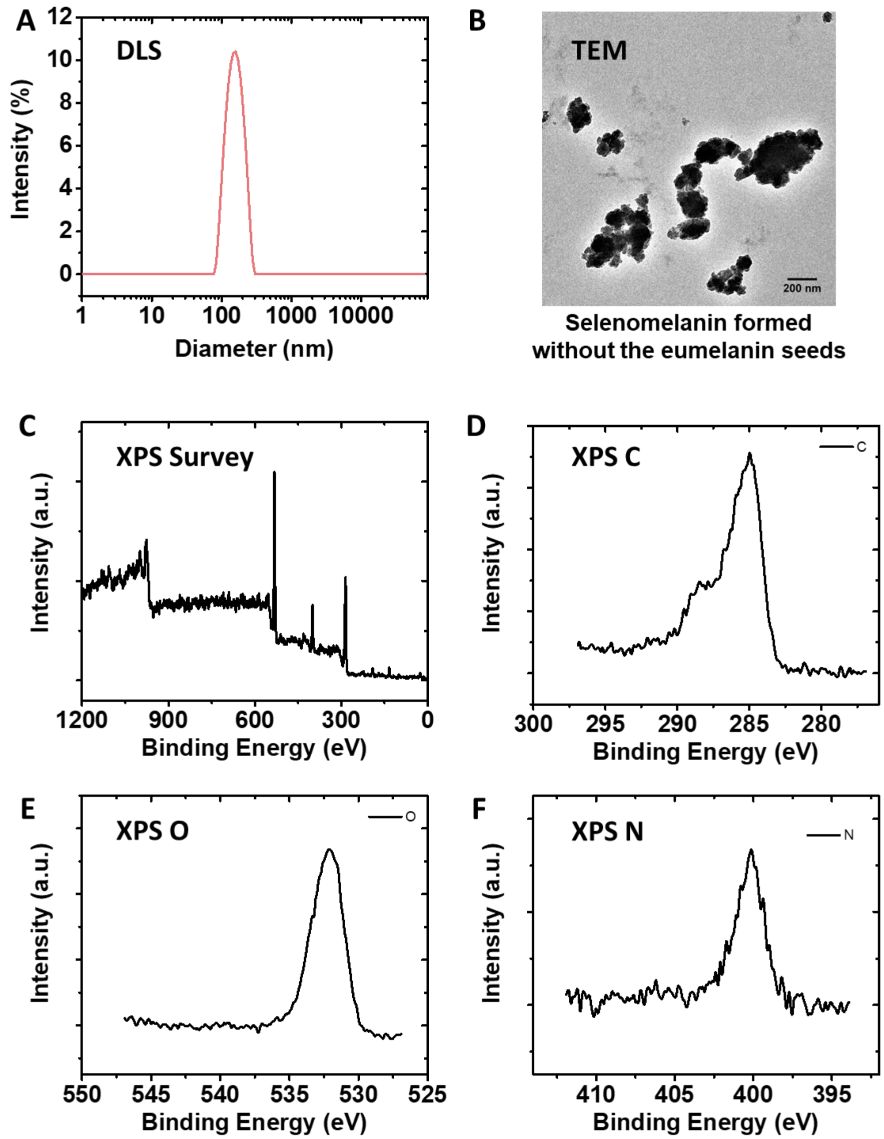

Fig. S1. Characterization of selenomelanin material. A. DLS intensity plot of SeNP sample in aqueous suspension. **B**. TEM image of selenomelanin formed without eumelanin seeds. Irregular morphology was observed. Samples were drop-casted onto copper grids and imaged without staining. **C**-**F**. XPS spectra of SeNP sample drop-casted onto a silicon substrate. **C**. Wide-scan survey spectra. **D**. C 1s spectrum. **E**. O 1s spectrum. **F**. N 1s spectrum.

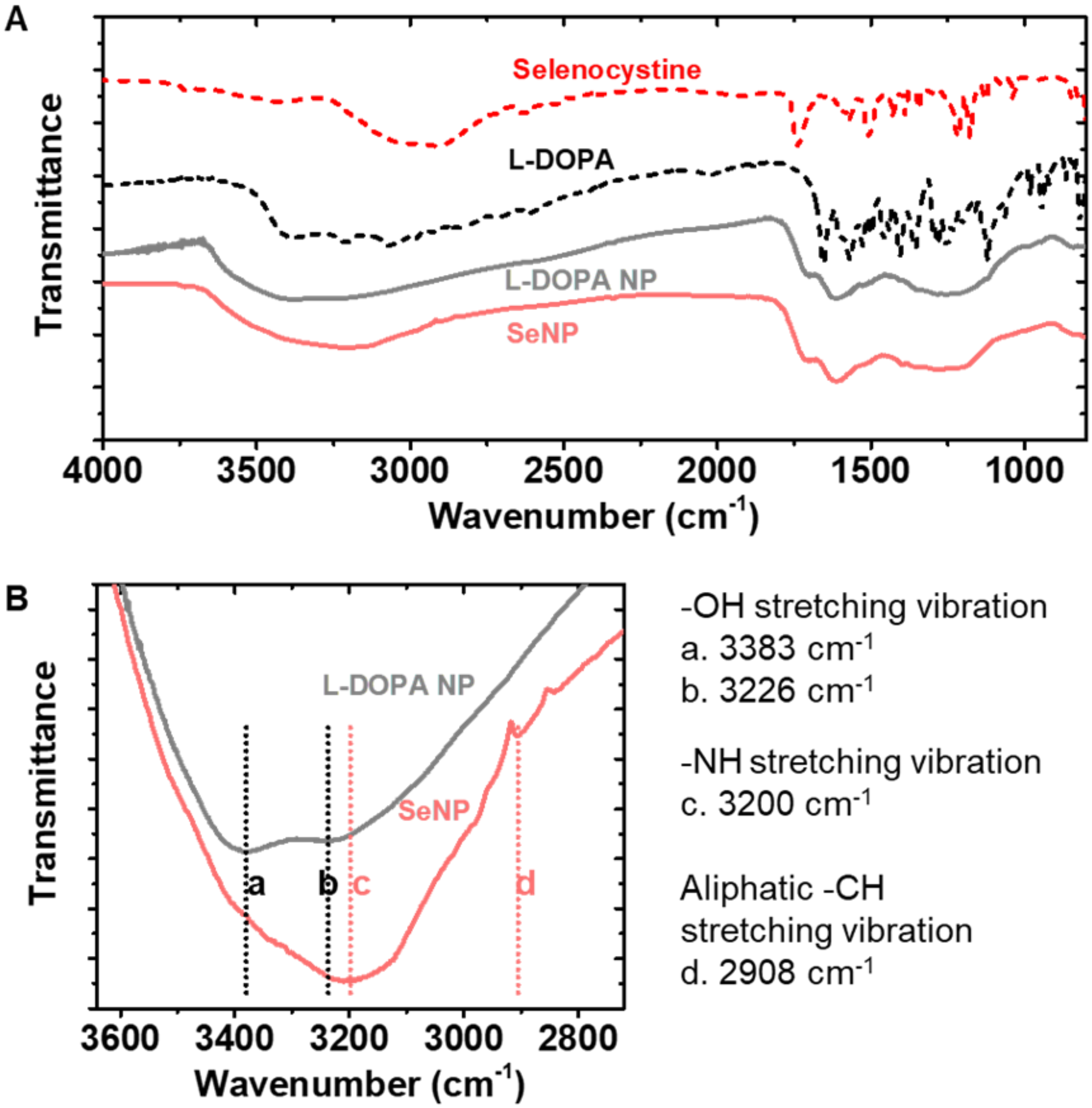

Fig. S2. FTIR spectra of L-DOPA NP, SeNP, and the monomer, L-DOPA and selenocystine. A. Full spectra. Dotted lines are the monomers, and solid lines are the NP samples. Y-axes are the offset transmittance of each sample. **B.** Zoomed spectra of SeNP and L-DOPA NP. Typical absorption bands were observed in SeNP sample at 3600-2400 cm^{-1} (stretching vibration of -OH, -COOH, -NH), 2908 cm^{-1} (stretching vibration of aliphatic -CH), 1715 cm^{-1} (stretching vibration of C=O from -COOH) and 1616 cm^{-1} (stretching vibration of $-NH_2$, bending vibrations of aromatic ring C=C).[8] The main differences between the SeNP with L-DOPA NP are the broad peak at 3600-2400 cm^{-1} and peak at 3200 cm^{-1} for SeNP in **B** (stretching vibration of -NH), while L-DOPA NP has two major peaks at 3383 and 3226 cm^{-1} (stretching vibration of -OH), which indicates that SeNP has more -NH groups as compared to L-DOPA NP. In addition, the 2908 cm^{-1} peak in SeNP suggested more aliphatic -CH is present, while for L-DOPA NP, the L-DOPA monomer cyclizes at a faster rate to produce DOPAchrome,[9] leading to very few aliphatic -CH in the polymeric NP.

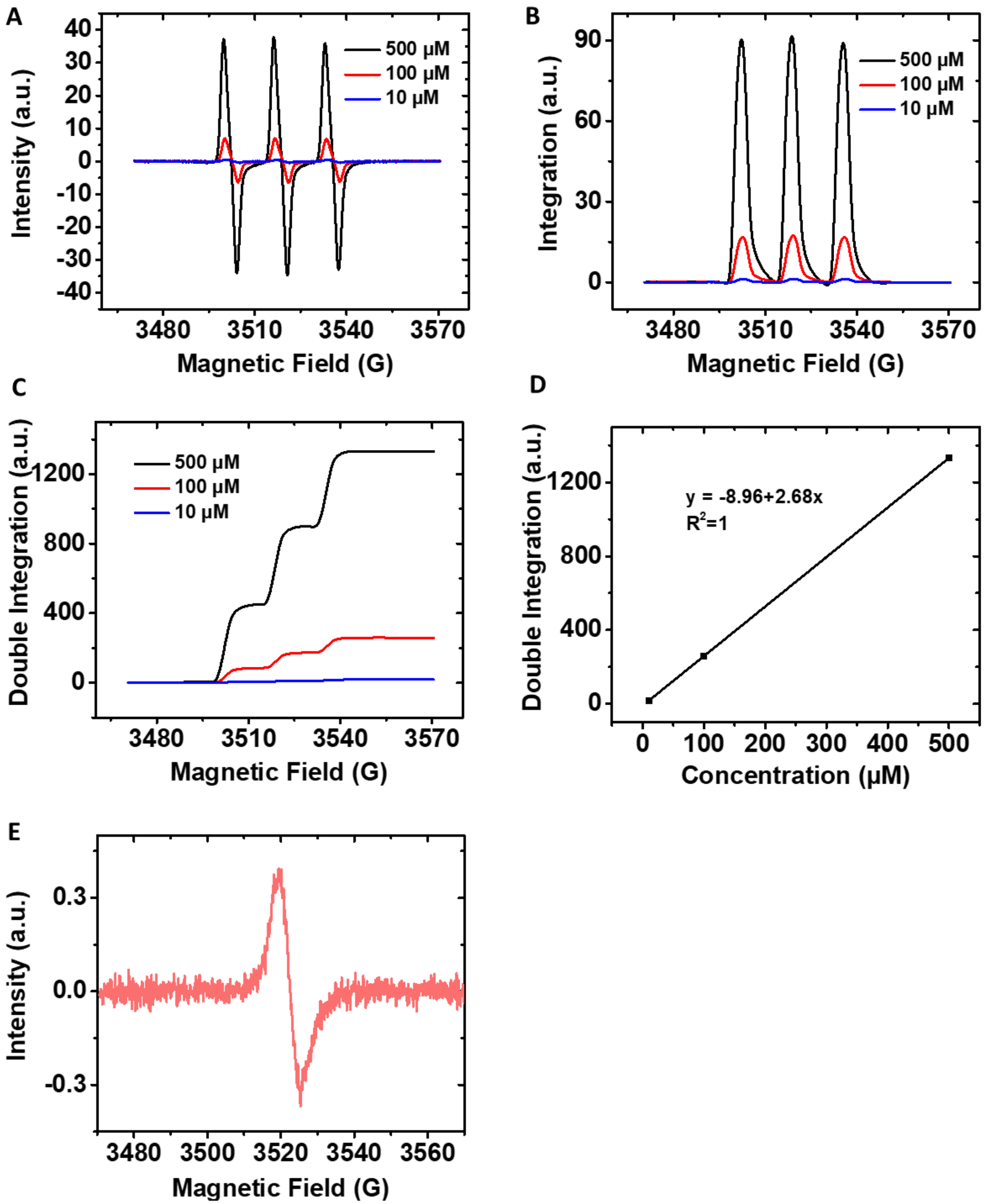

Fig. S3. EPR quantification of the radical content in SeNP. A. EPR sectra of 4-amino-TEMPO standard solutions of 500, 100 and 10 μM. **B**. Integration plots of EPR spectra in **A.** Plots were baseline corrected in Origin. **C**. Integrated EPR spectra of **B**. **D**. Calibration curve of double integration area *vs* spin concentration. **E**. EPR spectrum of 5.4 mg mL^{-1} SeNP aqueous suspension.

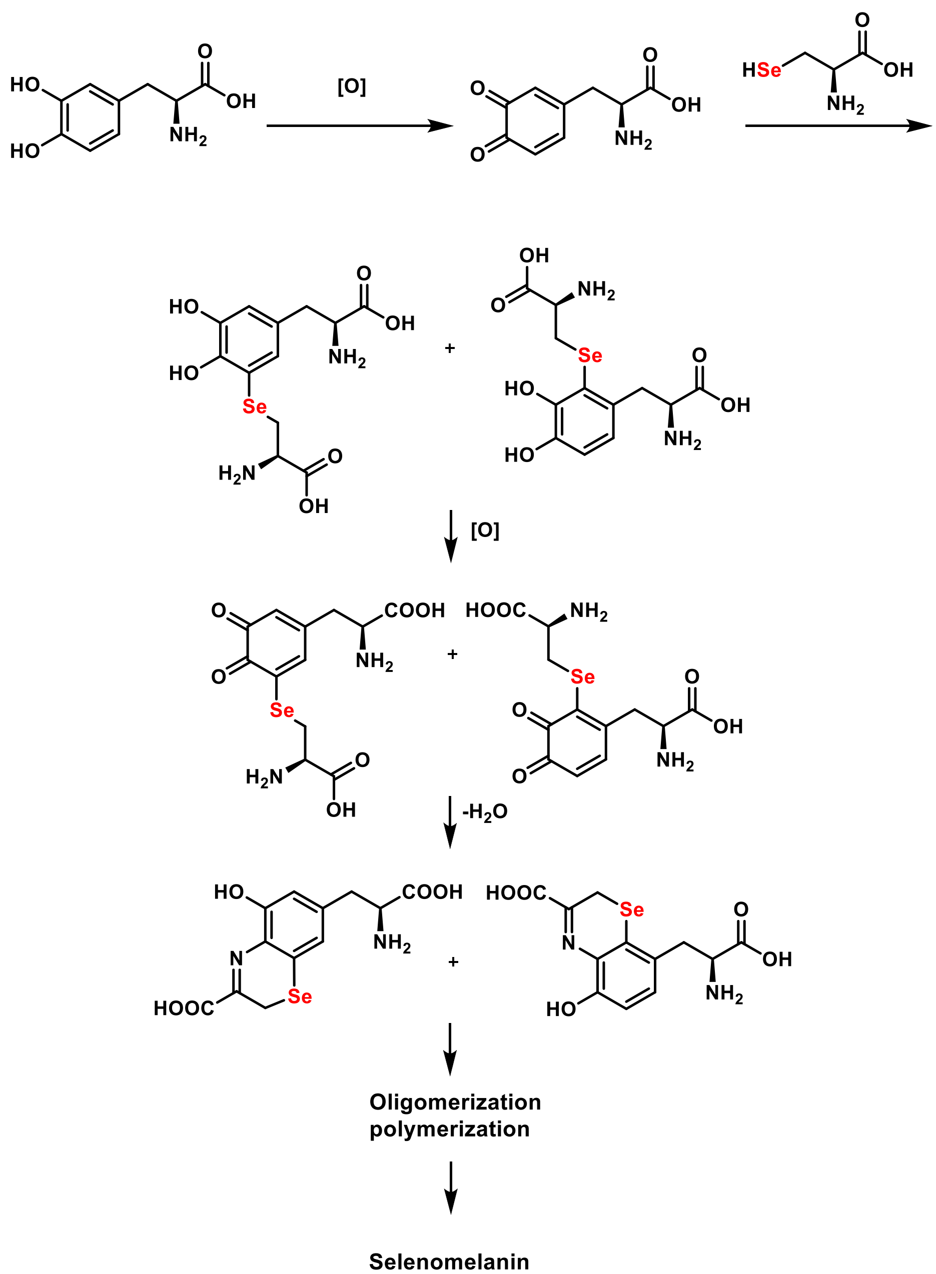

Fig. S4. Adapted Raper-Mason pathway for the formation of synthetic selenomelanin analogous to pheomelanin.[9]

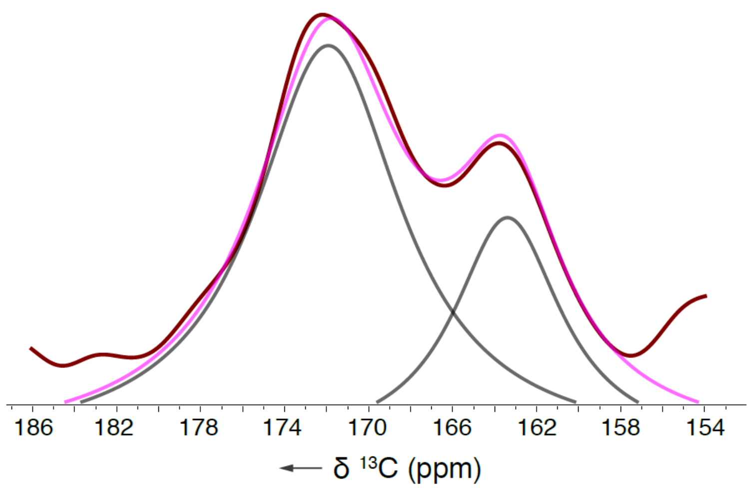

Fig. S5. ^{13}C ssNMR spectral integration in the COOH region of SeNP spectrum. The two peaks at 163 ppm (from selenocysteine) and 172 ppm (from L-DOPA) were deconvoluted and then integrated to determine the molar ratio of selenocysteine and L-DOPA to be 0.42:1.

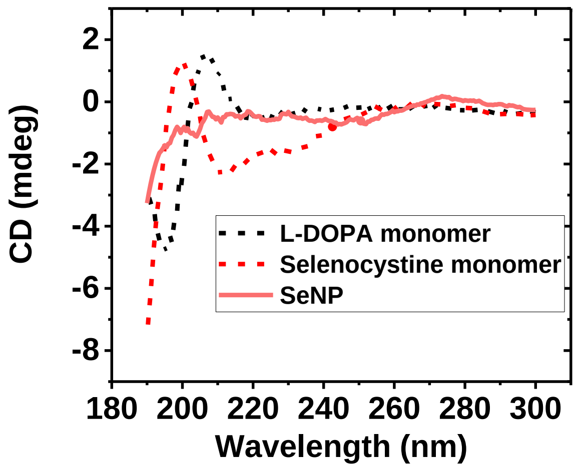

Fig. S6. Circular dichroism spectra of L-DOPA, selenocystine monomer, and SeNP. Both monomers have a CD signal, yet SeNP have little chiral signal. Disappearance of the CD signal suggested a change in chiral structures, consistent with the proposed cyclized subunits of SeNP.

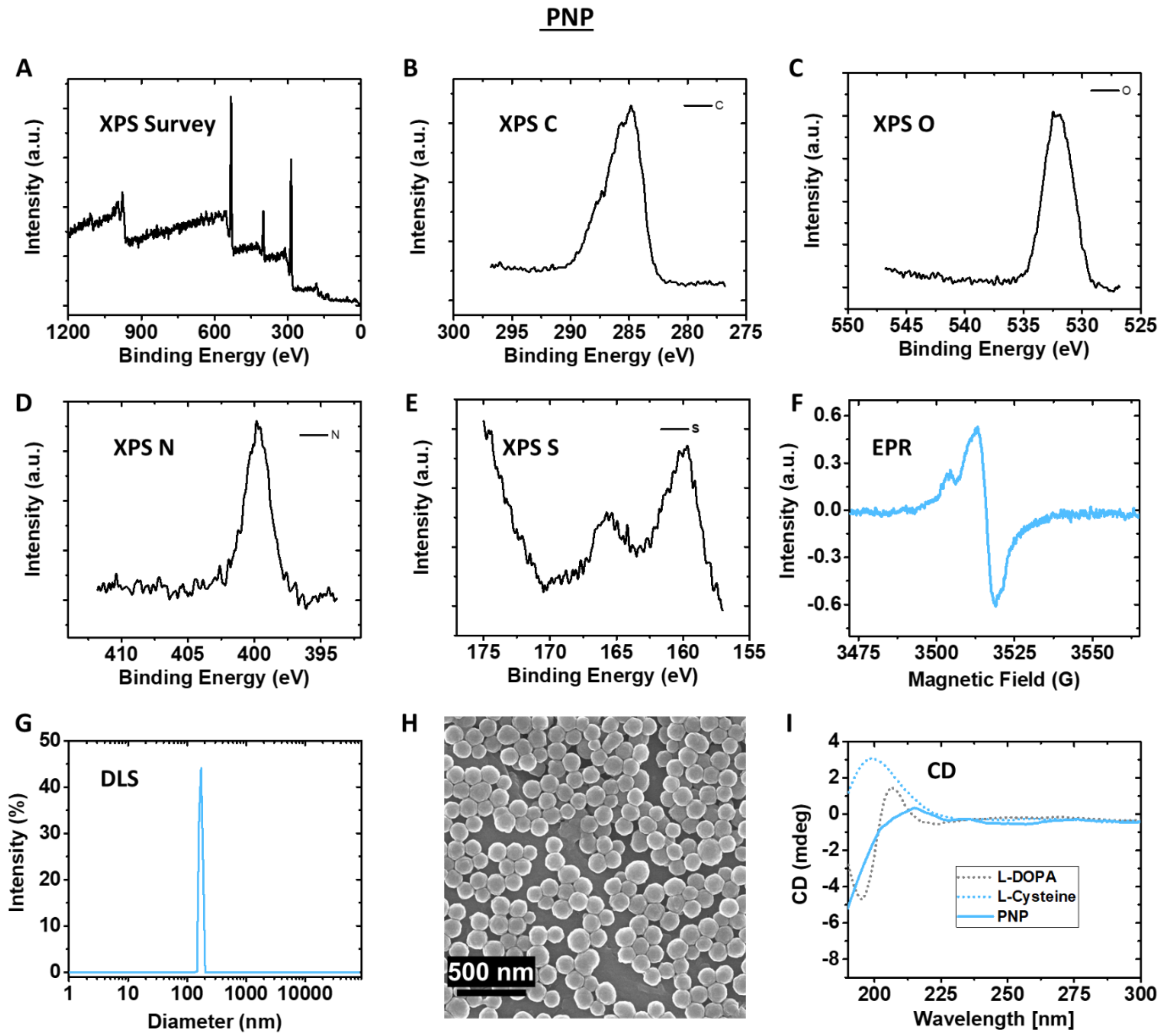

Fig. S7. Characterization of PNP. XPS spectra of PNP drop-casted onto a silicon substrate. **A**. Wide-scan survey spectrum. **B**. C 1s spectrum. **C**. O 1s spectrum. **D**. N 1s spectrum, **E**. S 2p spectrum. The S spectrum confirmed successful incorporation of sulfur from cysteine into the PNP product. **F.** EPR spectrum of PNP aqueous suspension. **G**. DLS intensity plot of PNP. **H**. SEM image of PNP. **I.** Circular dichroism spectra of PNP, L-DOPA, and cysteine monomers. The PNP sample has some chiral signal, corresponding to an open chain structure as indicated by the ssNMR of PNP in **Figure 2** of the main text.

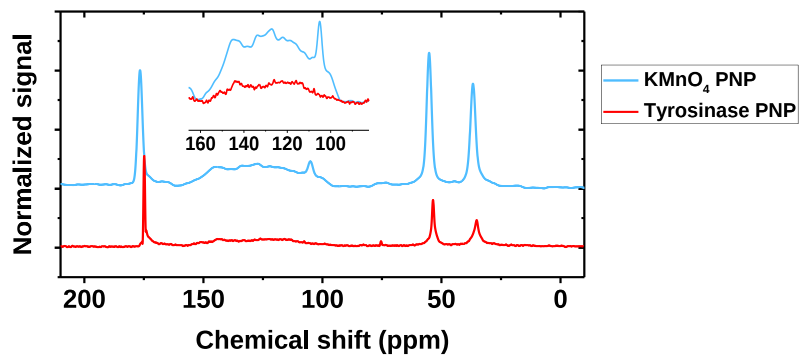

Fig. S8. Comparative ^{13}C ssNMR spectra of pheomelanin synthesized by both $KMnO_4$ (see main text also, Figure 2) or the enzymatic (tyrosinase) method. Red curve: ssNMR spectrum of pheomelanin mimic made by oxidation of L-DOPA and cysteine using tyrosinase as reported by Ito and coworkers.[10] Blue curve: Data for the chemical oxidation reaction as shown in the main text, **Figure 2**. Inset shows the zoomed aromatic regions.

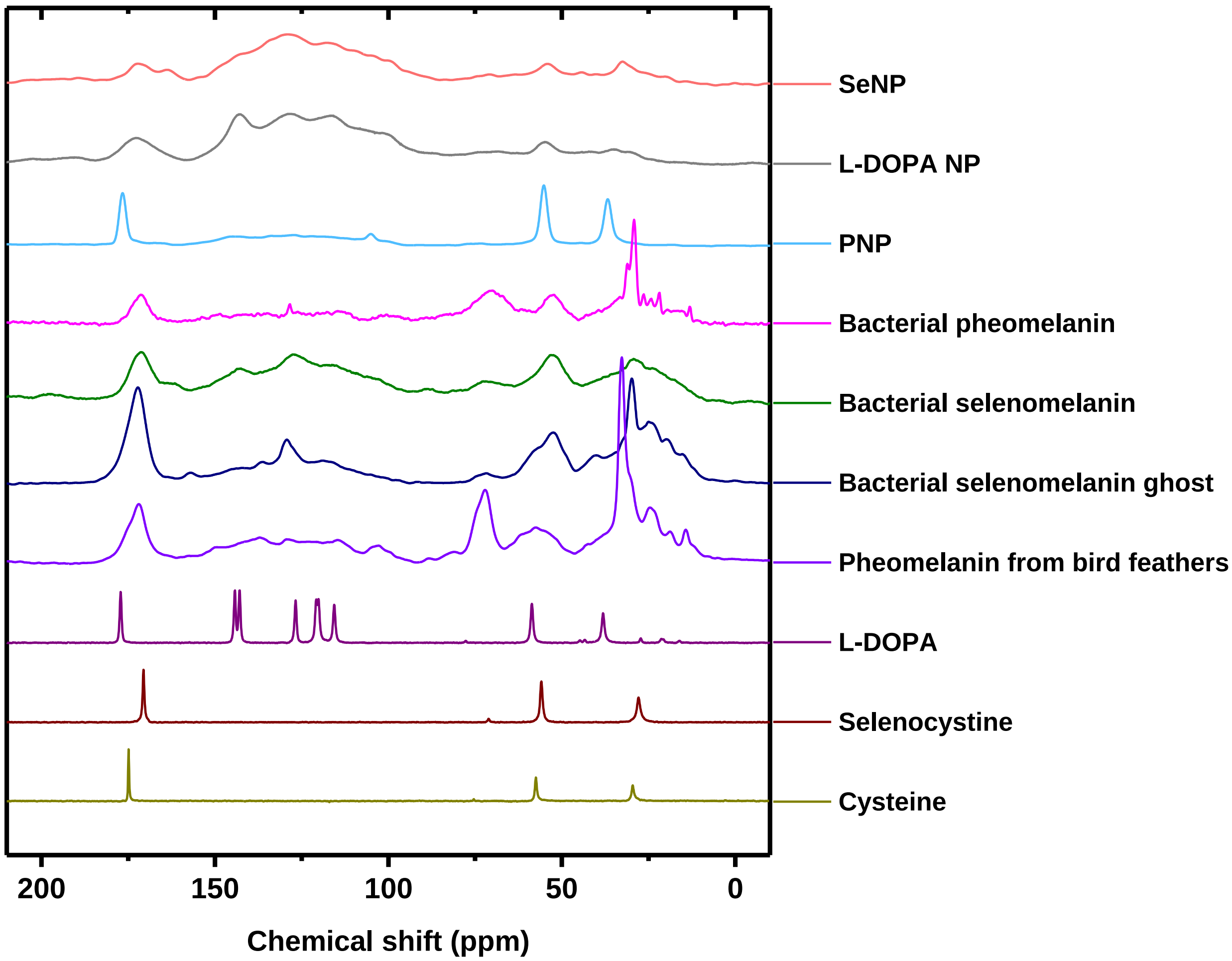

Fig. S9. ^{13}C ssNMR spectra of all the melanin and monomers used in this paper. Melanins include SeNP, L-DOPA NP, PNP, bacterial pheomelanin made by feeding L-DOPA and cysteine to *V. natriegens* (*vide infra*), bacterial selenomelanin and selenomelanin ghosts made by feeding L-DOPA and selenocystine to *V. natriegens* (*vide infra*), and natural pheomelanin extracted from covert feathers of a Rhode Island red rooster. Monomers include L-DOPA, selenocystine, and cysteine.

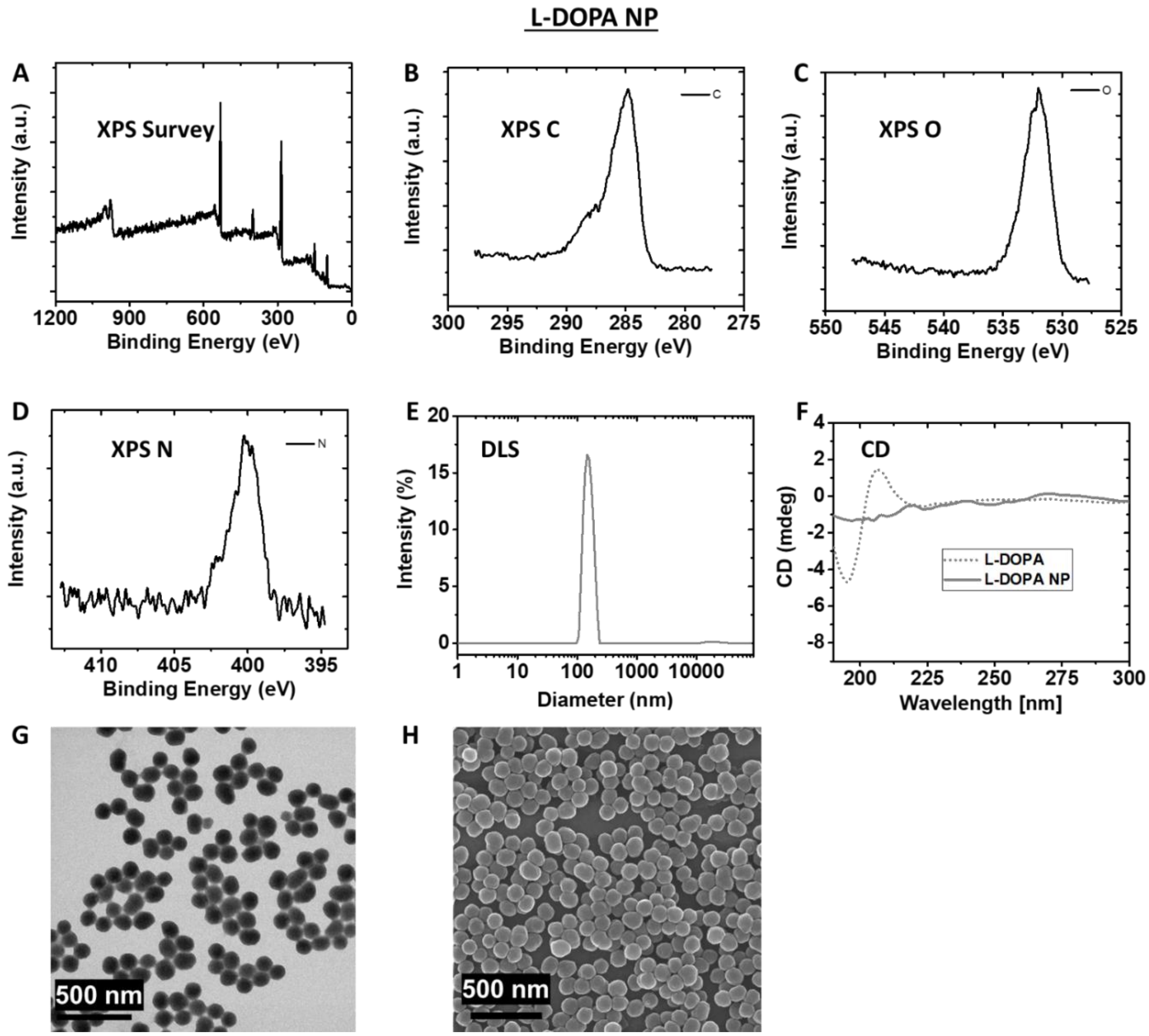

Fig. S10. Characterization of L-DOPA NP. A-D. XPS spectra of L-DOPA NP drop-casted onto a silicon substrate. **A**. Wide-scan survey spectrum. **B**. C 1s spectrum. **C**. O 1s spectrum. **D**. N 1s spectrum. **E**. DLS intensity plot of L-DOPA NP. **F**. Circular dichroism spectra of L-DOPA NP and L-DOPA monomer. The L-DOPA NP sample has no CD signal, suggesting most of the building blocks are 5,6-dihydroxyindole-2-carboxylic acid (DHICA). **G**. STEM image of L-DOPA NP. **H**. SEM image of L-DOPA NP

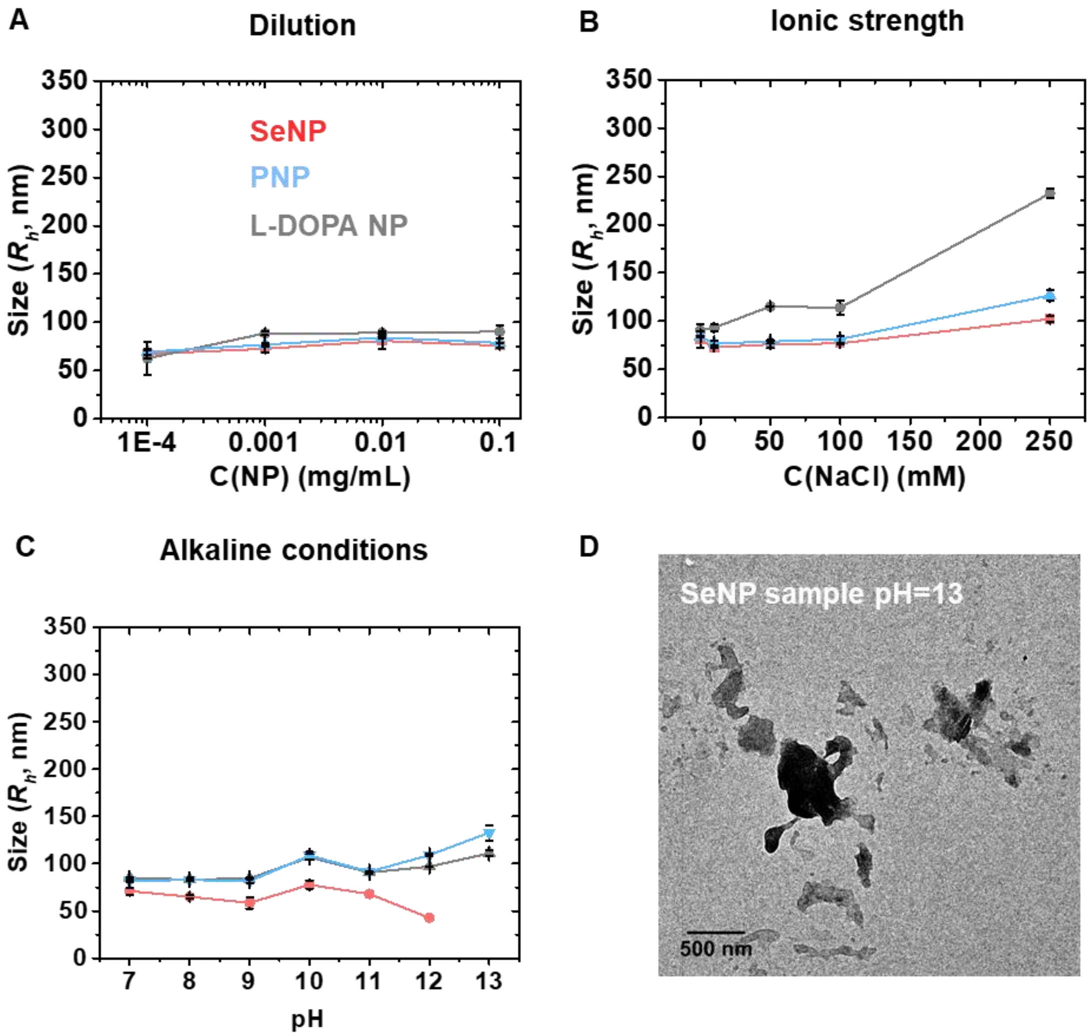

Fig. S11. Hydrodynamic radius measured by DLS of different NP under various conditions, and TEM analysis. A. NP dilution. **B**. Changing ionic strength (NaCl concentration). **C**. Increasing pH. Samples were measured in triplicate (n = 3). Error bars indicate s.d. First, all three types of NPs retained the same size at even 10^{-4} mg mL^{-1} concentration as shown by DLS (**A**). The high stability against dilution is probably because melanins are crosslinked by covalent/non-covalent interactions. Secondly, they behave differently against ionic strength and alkaline conditions. As shown in **B**, SeNPs experienced a much smaller size change under high ionic strength environments than L-DOPA NP. As 250 mM is relevant to biological applications,[11] this suggests that SeNP has good stability *in vitro*. Interestingly, SeNP was found to be soluble at pH>11. In contrast, similar solubility was not observed with PNP and L-DOPA. This is more evidence that SeNP are a good mimic for natural pheomelanin, as they were reported to be soluble under alkaline conditions due to their smaller molecular weight.[12] **D**. TEM image of SeNP sample in pH 13 buffer. Irregular aggregates were observed, with very few spherical particles, indicating that the SeNP are dissolved under alkaline conditions.

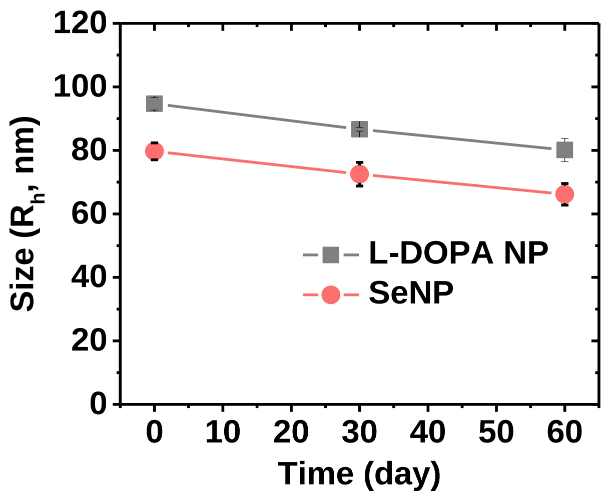

Fig. S12. Hydrodynamic radius change of L-DOPA NP and SeNP by DLS over 60 days under ambient conditions. The data indicate good stability during the experimental conditions, which can be attributed to the low zeta potential of about −20.3 mV that leads to strong electrostatic repulsions (Table S1). No large aggregates were formed in SeNP. Only minimal hydrodynamic radius decrease was observed. The trend is the same with L-DOPA NP, yet the reason for the slight size decrease is unclear.

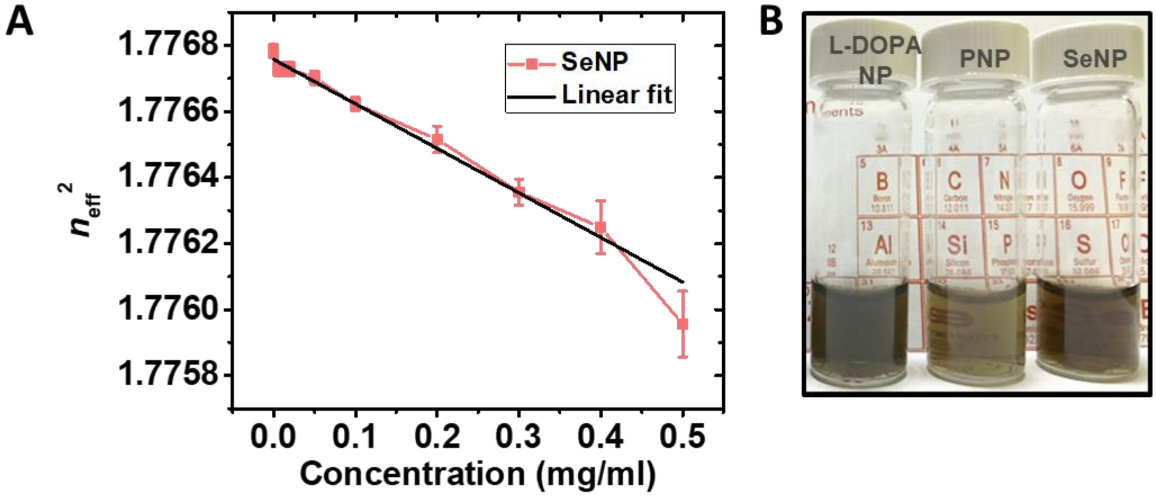

Fig. S13. Refractive index measurement of the SeNP sample. RI=1.3323. **B**. Optical image of the different nanoparticle solutions at 0.1 mg mL^{-1} in ultrapure water: polydopamine (PDA), L-DOPA NP, PNP, SeNP. The RI measured for SeNP is low compared to current eumelanin NPs which are higher than 1.7.[13, 14] This is consistent with natural pheomelanin and is mostly due to the lack of pi stacking which commonly happens in DHI and DHICA structures of eumelanin.

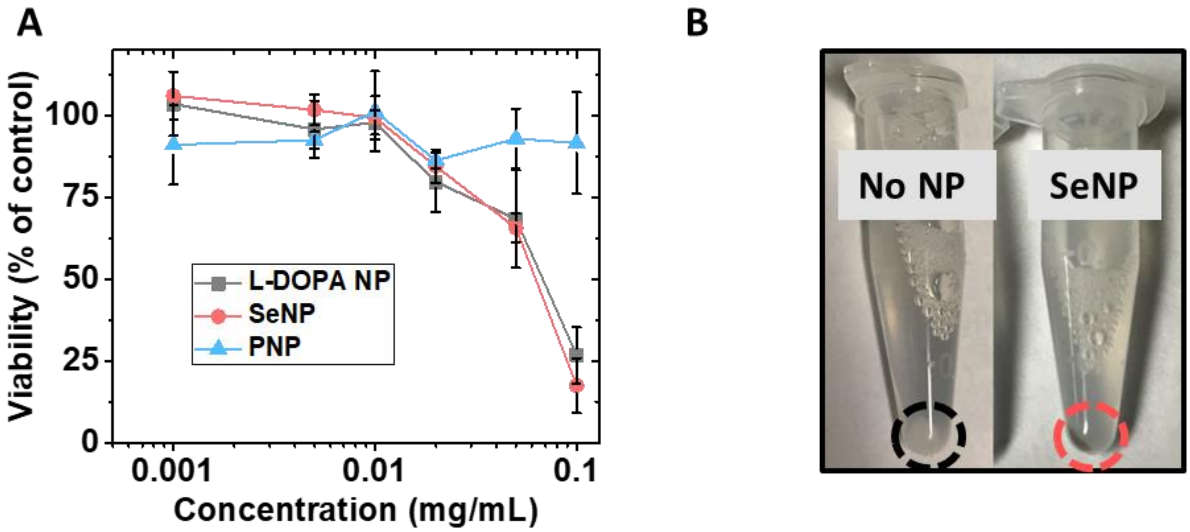

Fig. S14. Biocompatibility studies of the SeNP, PNP and L-DOPA NP. A. Cell viability of NHEK cells after incubation with NPs for 24 h. Viability was determined using the CellTiter-Blue® assay. **B**. Cell pellet images of NHEK cells treated with no NP (left), and SeNP (0.004 mg mL^{-1}) (right). The dark pellet indicates uptake of the SeNP into the NHEK cells.

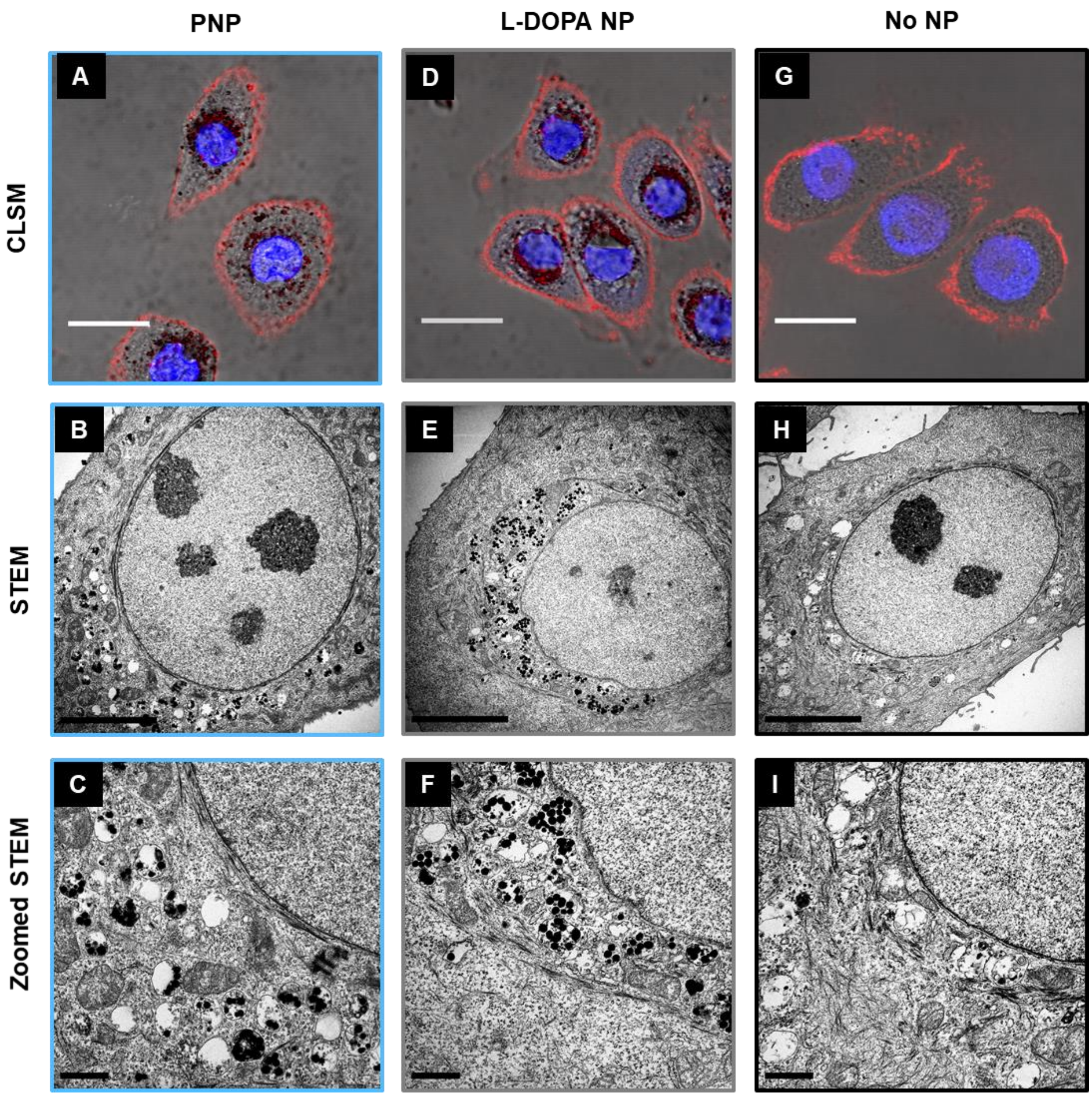

Fig. S15. Subcellular distribution of different NPs in NHEK cells. Cells treated with PNP, L-DOPA NP, or No NP for 24 h, then imaged *via* live-cell CLSM and STEM. **A, D, G**. CLSM images of NHEK after treatment, or control. Cell membrane stained with WGA (red) and nuclei stained with Hoechst 33342 (blue). Scale bar 20 μm. **B, C, E, F, H, I**. STEM micrographs. Samples were prepared by flat, resin-embedding cells in monolayer cell culture and sectioning. The images were acquired by high-angle annular dark-field imaging (HAADF) and contrast-inverted to reflect the appearance of standard TEM imaging. **C, F, I** (scale bar 1 μm) show higher magnification of the perinuclear region in **B, E, H** (scale bar 5 μm).

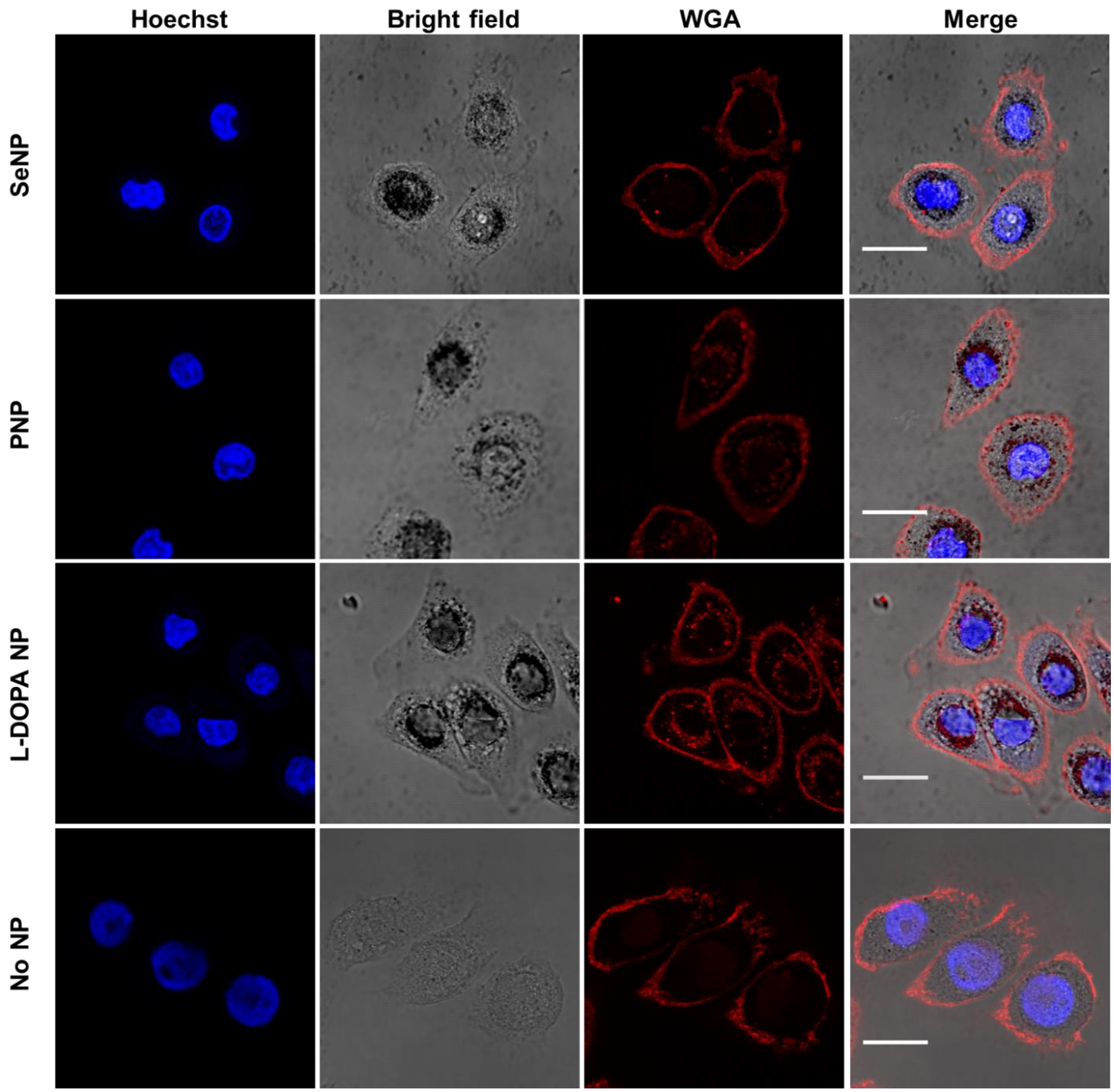

Fig. S16. Single channel CLSM images of NP-treated cells. NHEK cells were incubated with SeNP, PNP, or L-DOPA NP for 24 h and stained with Hoechst 33342 (blue) or WGA (red). Scale bar 20 μm.

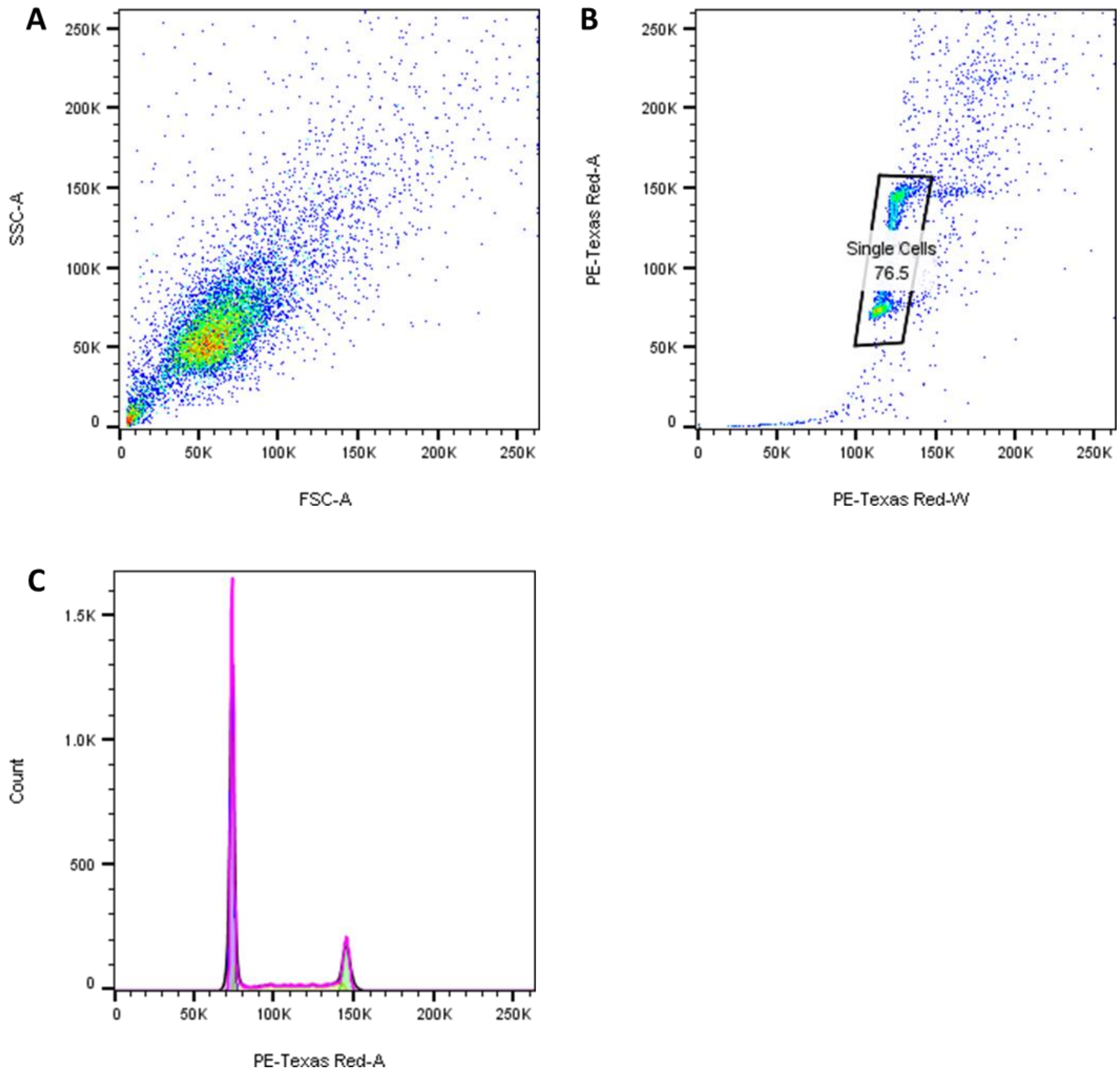

Fig. S17. Flow cytometry data analysis workflow using FlowJo software. A. NHEK cell population. **B**. Singlet gate using PE-Texas Red area vs width. **C**. Histogram of PI counts (PE-Texas Red channel) used for cell cycle analysis in FlowJo software.

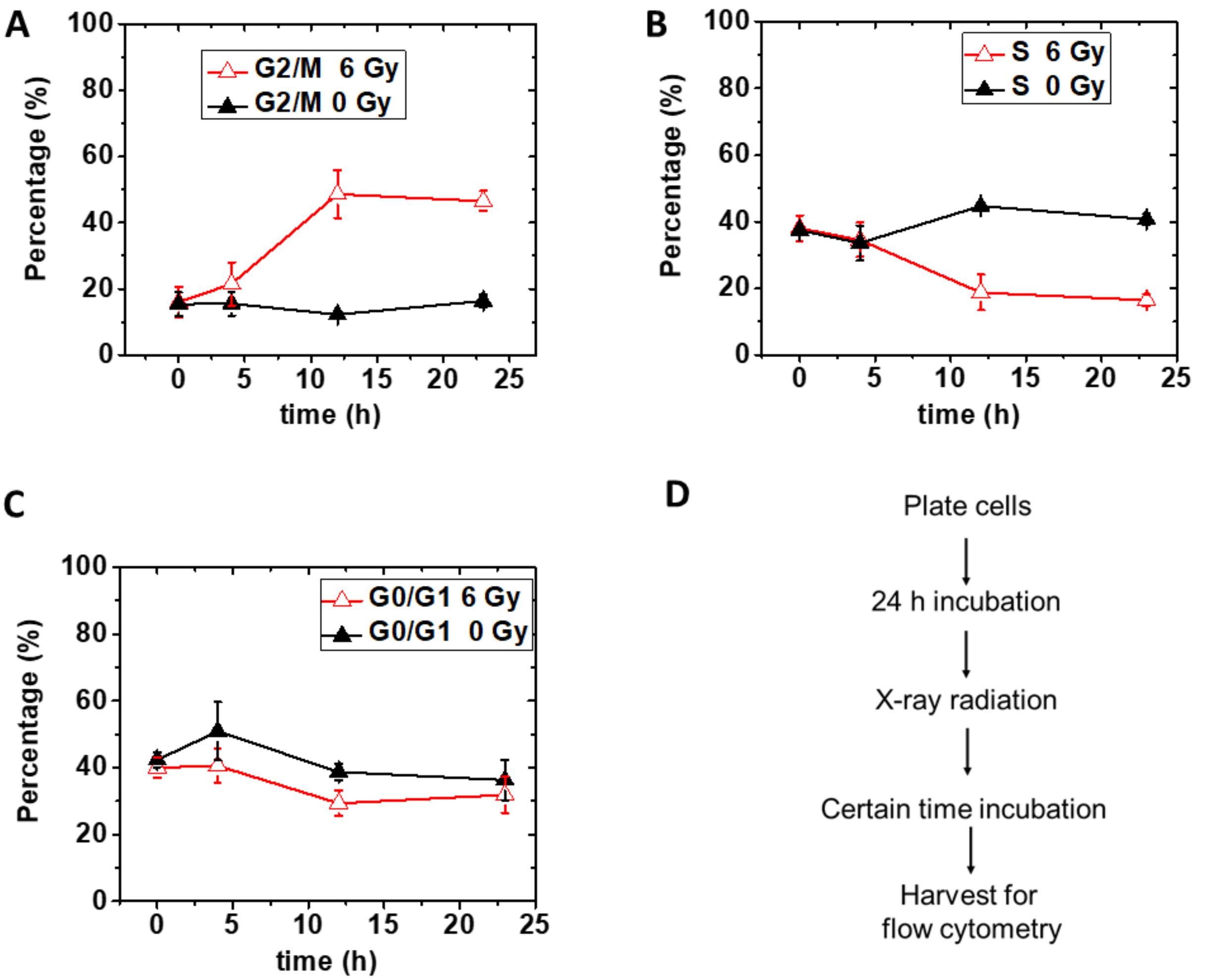

Fig. S18. Cell cycle changes of NHEK cells induced by X-ray irradiation. The cell population percentage in different cell cycle phases, **A**. G2/M, **B**. S, and **C**. G0/G1 were plotted against post-irradiation time. **D**. Experimental timeline for this initial study.

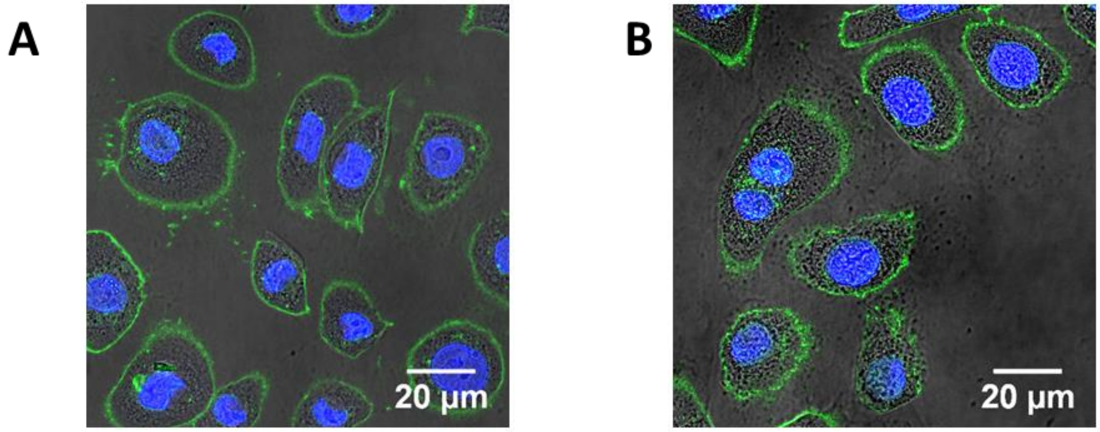

Fig. S19. NHEK cell morphology before (A) and after (B) X-ray irradiation. Bright field images overlaid with fluorescent channels for WGA (green) and DAPI (blue).

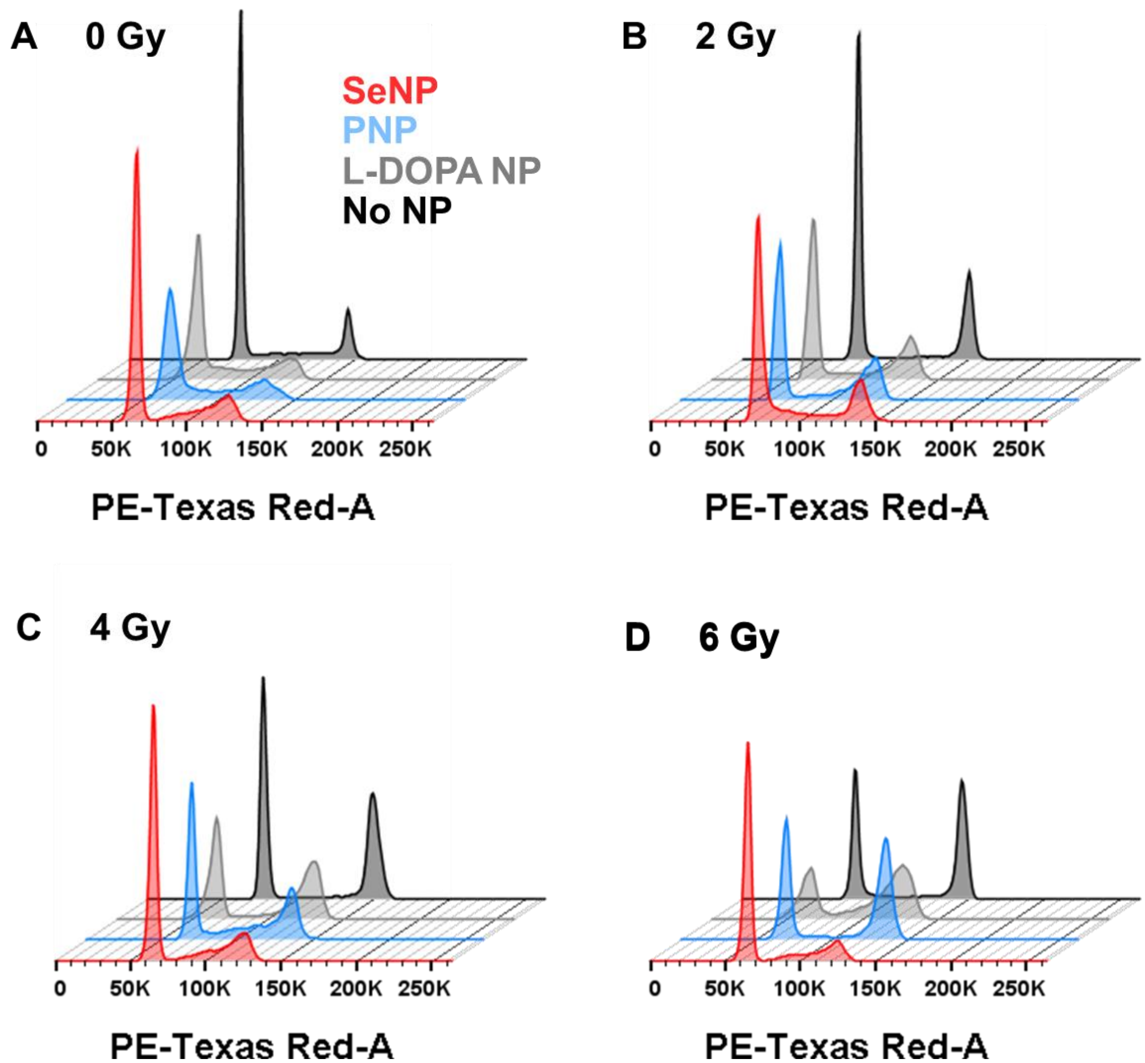

Fig. S20. Cell cycle distribution plots of cells treated with different NPs followed by X-ray irradiation with different doses. **A**. 0 Gy. **B**. 2 Gy. **C**. 4 Gy. **D**. 6 Gy. Red=SeNP. Blue=PNP. Gray=L-DOPA NP. Black=No NP control. Each histogram is offset for better clarity and is representative of three independent experiments.

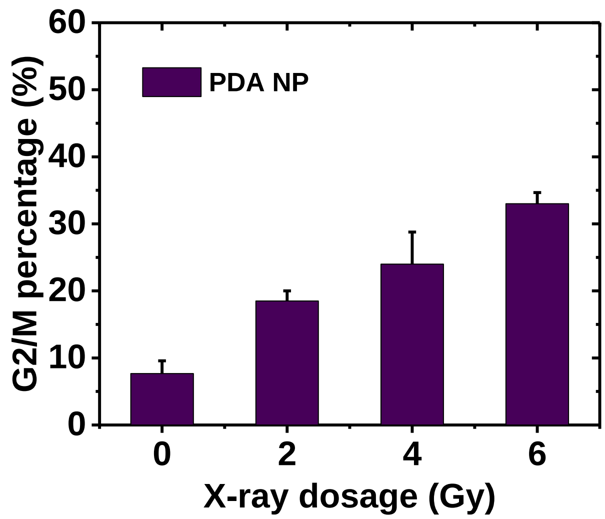

Fig. S21. Cell cycle distribution of cells treated with PDA NP followed by X-ray irradiation with different doses. Cells were incubated with PDA NP (0.004 mg mL^{-1}) for 24 h then irradiated with X-rays. All other conditions are identical for SeNP, PNP and L-DOPA NP. PDA was synthesized by standard oxidation in air under alkaline conditions.[15]

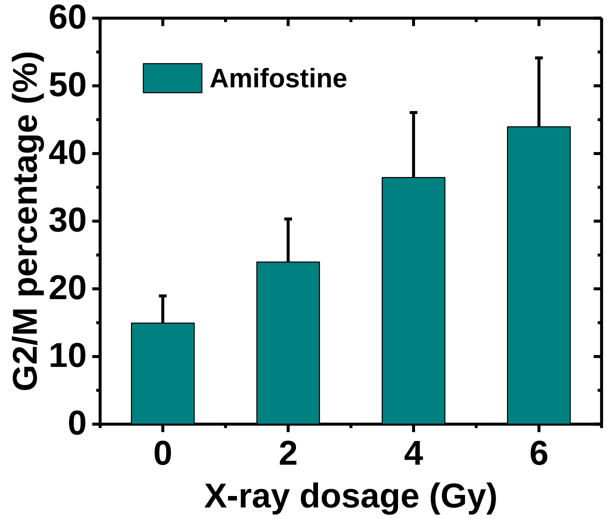

Fig. S22. Cell cycle distribution of cells treated with Amifostine followed by X-ray irradiation with different doses. Cells were incubated with Amifostine (2 mg/mL) for 1 h then irradiated with X-ray. The dosage of Amifostine was chosen according to a previous paper.[16] Amifostine works by scavenging reactive oxygen species. Our result suggests no protection against the cell cycle arrest caused by X-ray.

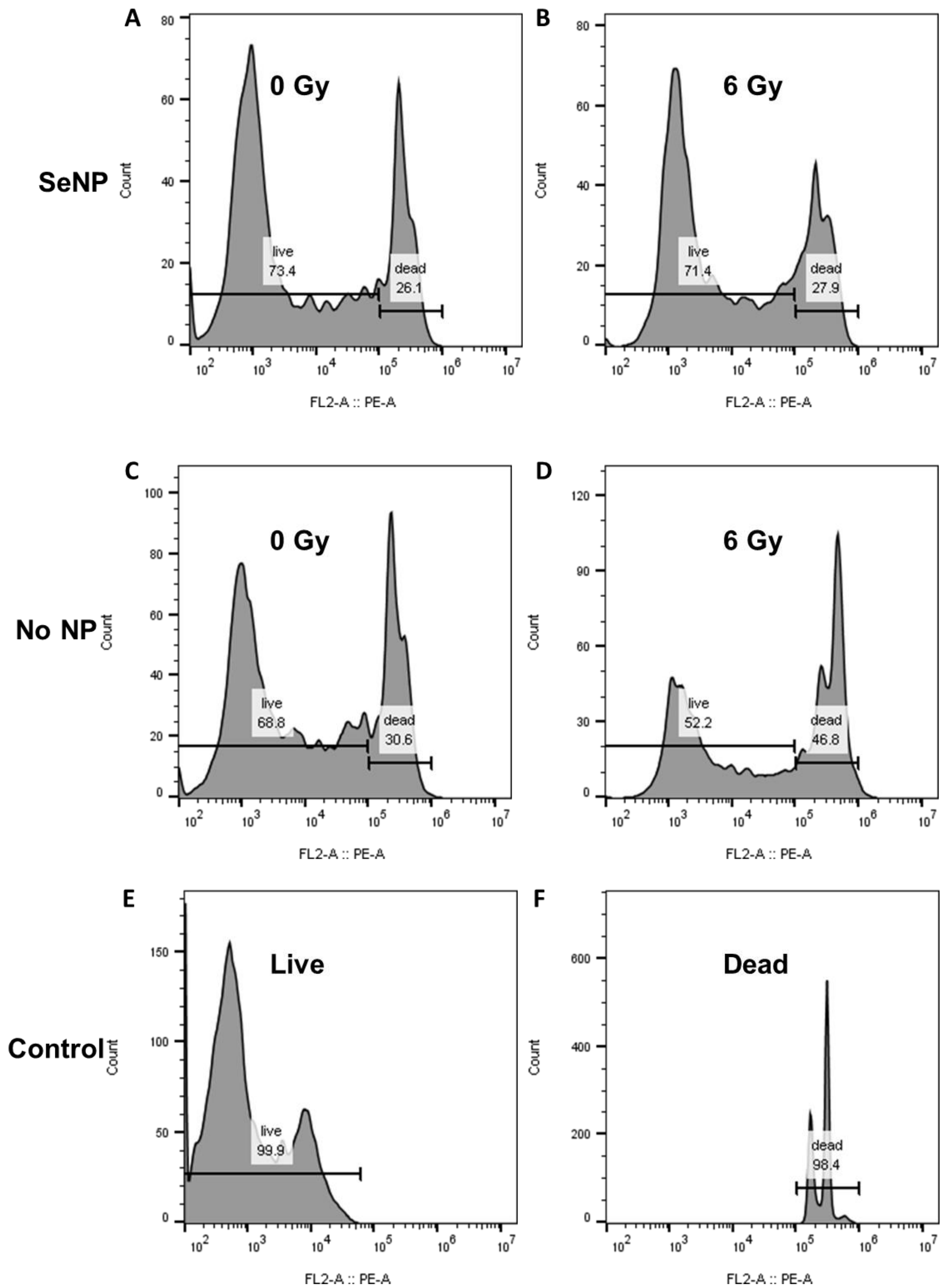

Fig. S23. NHEK cell viability tested using flow cytometry. For this experiment, cells were treated with or without SeNP, irradiated with 6 Gy or 0 Gy X-ray, and incubated for 24 h. Then the cells were harvested and washed with DPBS. A PI solution (0.5 μL, 1 mg mL^{-1} in PBS) was added and cells were incubated on ice for 15 minutes prior to live cell flow cytometry measurements. Cells were treated with SeNP (0.004 mg mL^{-1}) followed by 0 Gy (**A**) or 6 Gy (**B**) X-ray irradiation, or no particles followed by 0 Gy (**C**) or 6 Gy (**D**) X-ray irradiation. NHEK cells without PI stain were used as a live control (**E**). Cells fixed with 70% ethanol and stained with PI were used as dead cell control for cell gating (**F**).

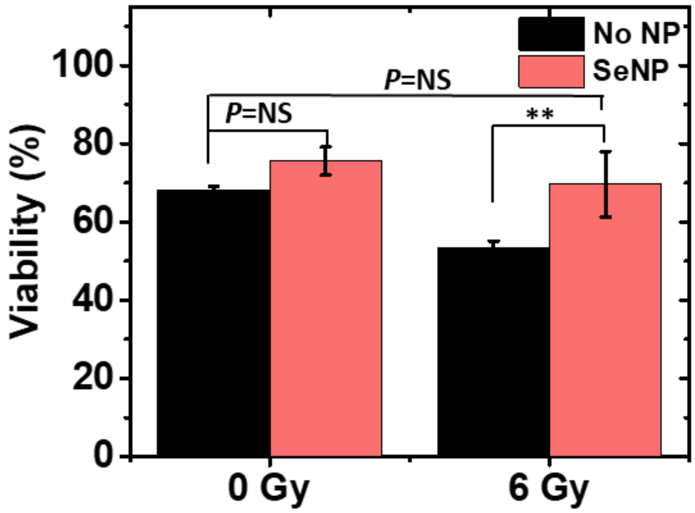

Fig. S24. NHEK cell viability using flow cytometry. Cells were treated with and without SeNP, followed by 6 Gy or 0 Gy X-ray irradiation and then incubated for 24 h. Red= SeNP. Black=No NP control. 6 Gy X-ray significantly decreased the cell viability of the non-NP treated cells (*P*= 0.00015), while SeNP treatment increased the viabilty of the irradiated cells to approximately the same value as the non-irradiated control group (0 Gy, no NP) (*P*=0.78). SeNP treatment did not change the viability of non-irradiated cells at this concentration (0.004 mg mL^{-1}) (*P*=0.024), which is consistent with the CellTiter-Blue® viability assay. NS represents *P*>0.01.

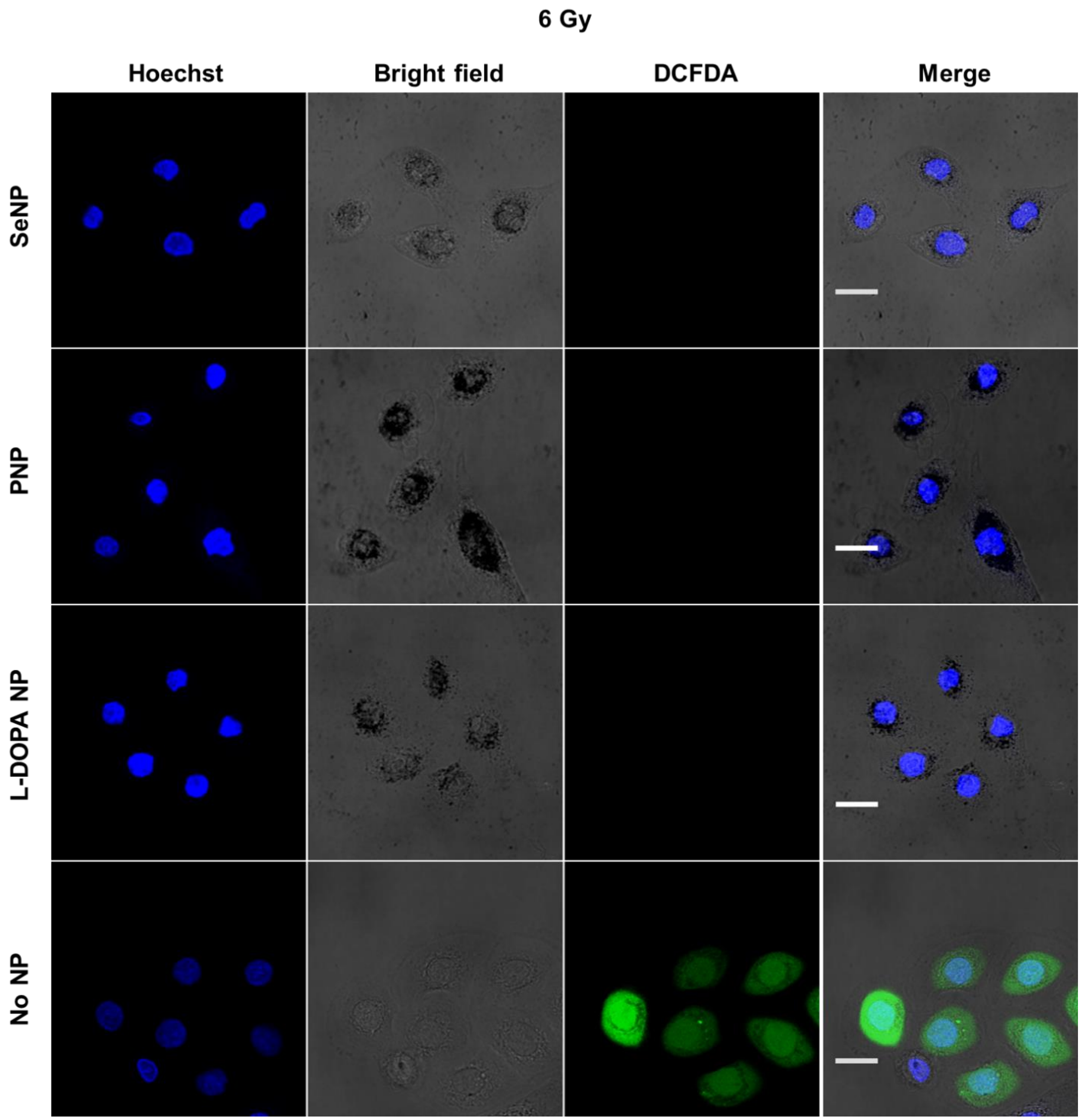

Fig. S25. Single channel CLSM images of cells irradiated with 6 Gy X-ray. ROS scavenging in NP-treated NHEK cells after 6 Gy X-ray irradiation, stained with Hoechst 33342 (blue) and fluorogenic ROS probe DCFDA (green). Scale bars 20 μm.

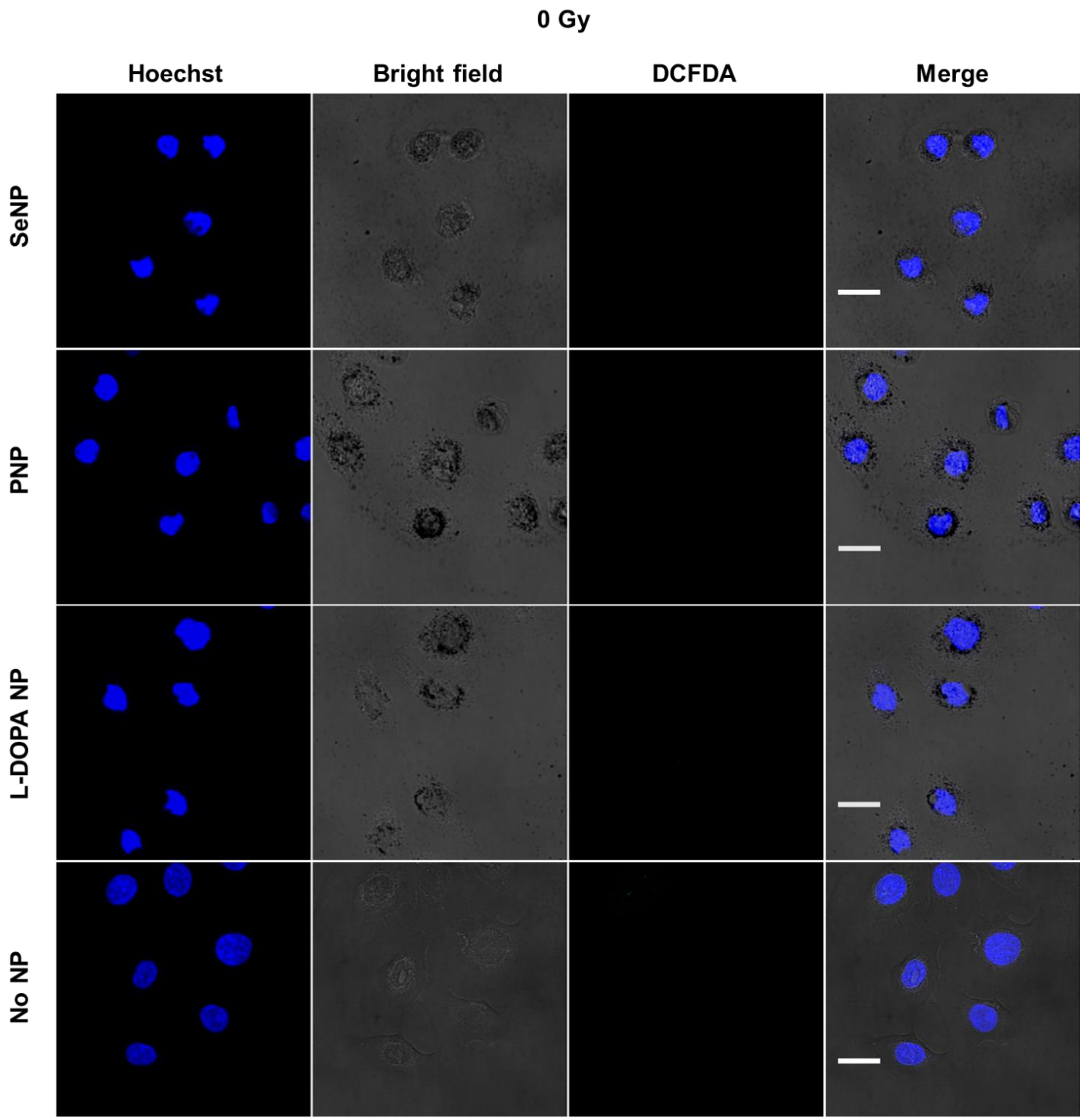

Fig. S26. Single channel CLSM images of non-irradiated cells. ROS scavenging in NP-treated NHEK cells with no X-ray irradiation, stained with Hoechst 33342 (blue) and ROS DCFDA probe (green). Scale bars 20 μm.

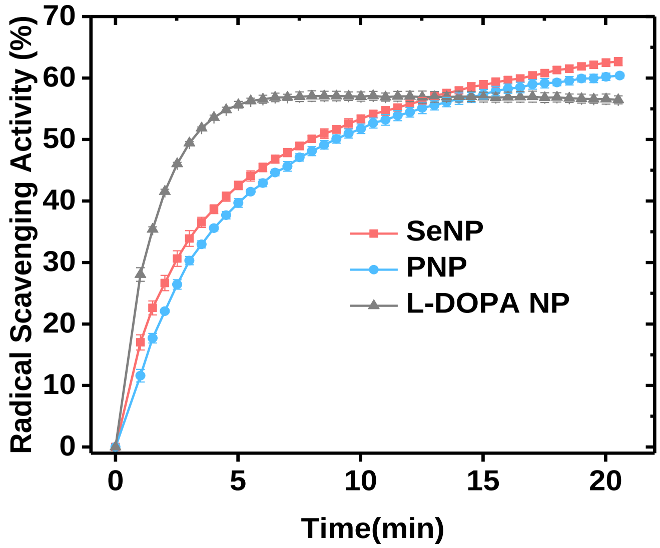

Fig. S27. DPPH assay for antioxidant activity of SeNP (red), PNP (blue) and L-DOPA NP (gray). Error bars represent the standard deviation of triplicate studies. For SeNP and L-DOPA NP, the error bars are too small to be seen.

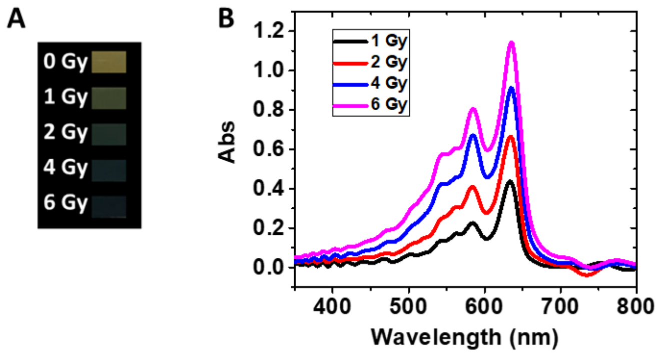

Fig. S28. X-ray GAFCHROMIC EBT3 film experiments to evaluate the physical shielding of different NPs. The X-ray films were cut into 4 mm×40 mm sections, placed underneath a 2 mL NP suspension (1 mg mL^{-1}) in a capless 8 mL scintillation vial, irradiated from above, and subsequently measured in a quartz cuvette using a UV-Vis spectrometer. **A**. Coloration of EBT3 film after different doses of X-ray irradiation. **B**. UV-Vis spectra of the corresponding films. **C**. Absorbance values at 635 nm for several X-ray doses.

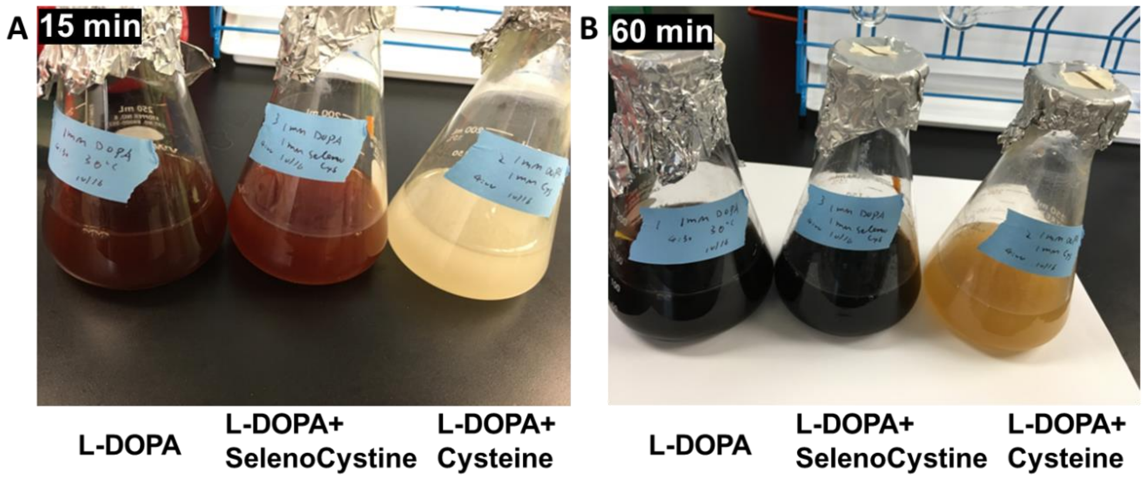

Fig. S29. Color change during the biological synthesis of selenomelanin. A. Image of *V. natriegens* culture media 15 min after monomer addition. **B**. Image of the *V. natriegens* culture media 60 min after monomer addition.

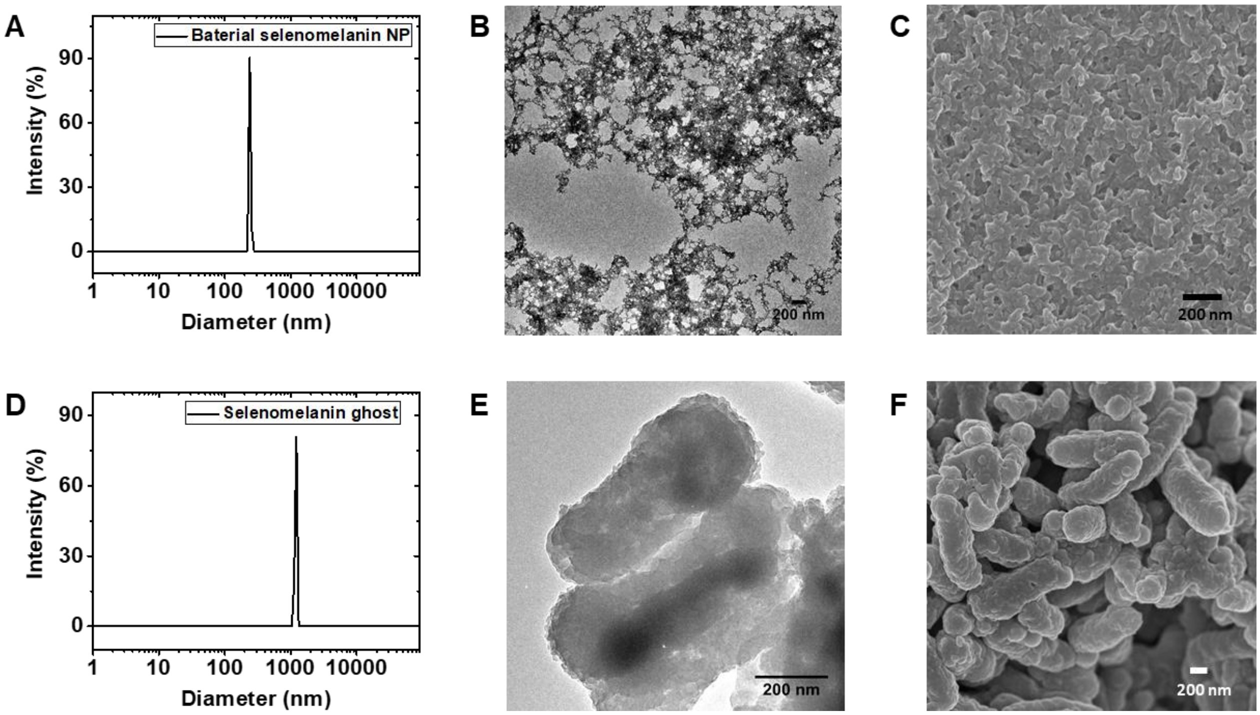

Fig. S30. DLS, TEM, and SEM of selenomelanin NPs and ghosts made by *V. natriegens*. A. B. C. are the DLS plot, TEM image and SEM image of the nanoparticles made by *V. natriegens* in the supernatant, respectively. **D. E. F**. are the DLS plot, TEM image and SEM image of the micrometer-sized selenomelanin ghosts after purification, respectively. Scale bar 200 nm.

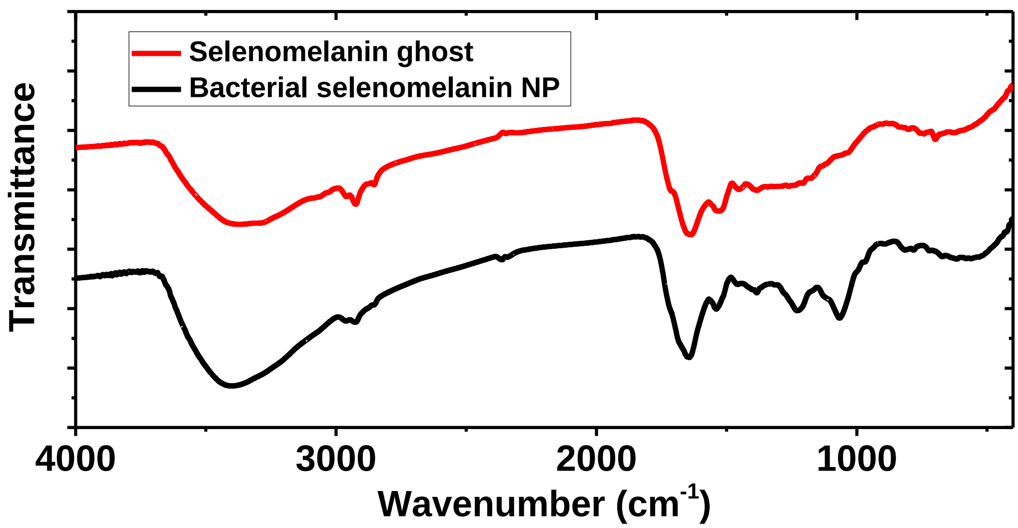

Fig. S31. FTIR spectra of selenomelanin made by *V. natriegens*. Bacterial selenomelanin NP is the nanoparticles made by bacteria in the supernatant. Selenomelanin ghost is the ghost after purification.

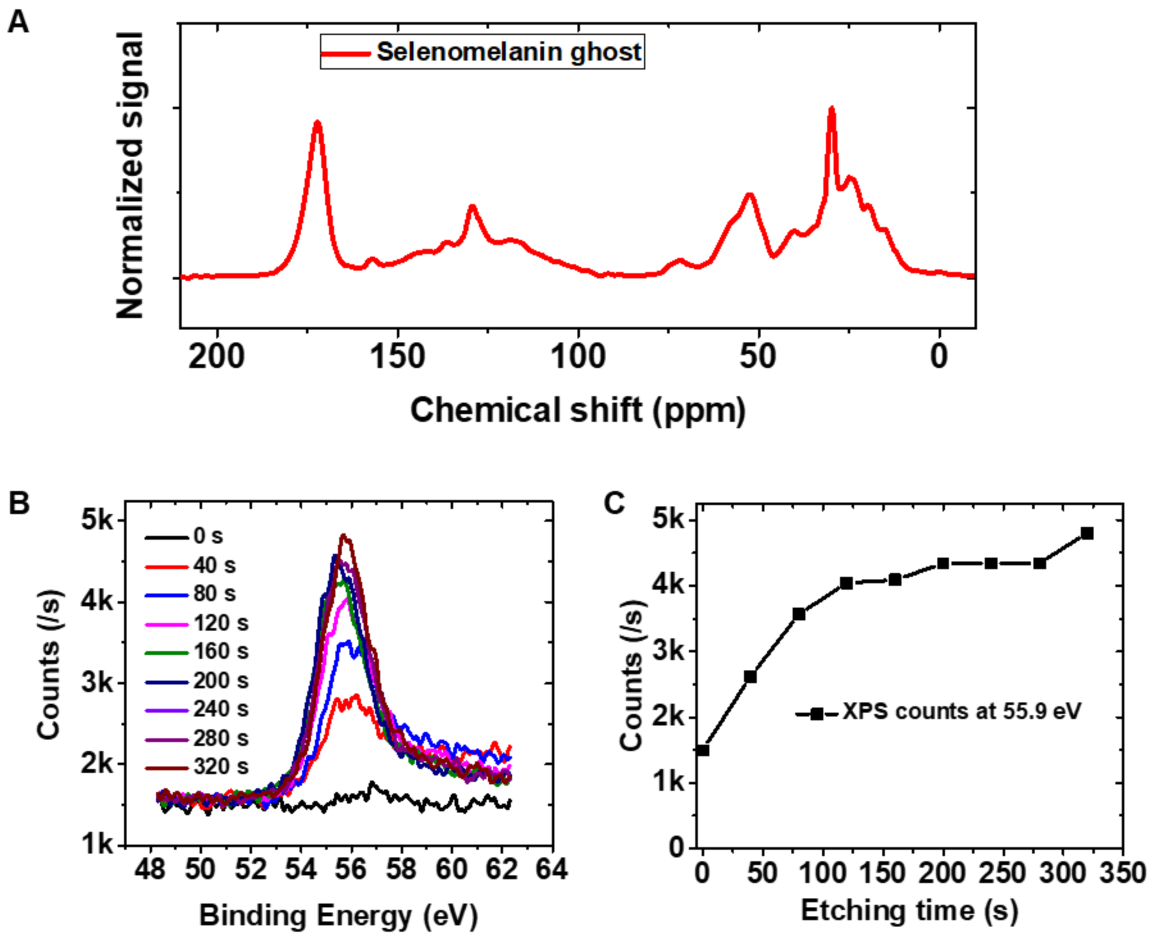

Fig. S32. Characterization of selenomelanin ghosts. **A**. ^{13}C ssNMR spectrum of selenomelanin ghosts. **B**. XPS Se3d spectrum of selenomelanin ghosts drop-casted onto a silicon substrate after different ion beam etching times. **C**. Se 3d spectra after different beam etching times.

Table S1. Statistical analysis for **Figure 3E** of the main text. Cell population percentage in G2/M phase after X-ray irradiation. Student's two-tailed t-tests were performed in Excel.

		G2/M population (%)		Student's T test	
	X-ray dosage	Average	s.d.	*P*	Significance
SeNP	0 Gy	13.8	3.9	0.70	NS
	2 Gy	15.3	3.6	0.00037	***
	4 Gy	15.9	4.5	3.1E-7	******
	6 Gy	16.8	9.0	3.0E-5	****
PNP	0 Gy	17.4	4.8	0.11	NS
	2 Gy	23.0	4.0	0.33	NS
	4 Gy	36.8	3.1	0.36	NS
	6 Gy	44.2	4.5	0.56	NS
L-DOPA NP	0 Gy	11.5	5.6	0.10	NS
	2 Gy	22.5	4.5	0.28	NS
	4 Gy	38.3	6.7	0.99	NS
	6 Gy	41.9	7.5	0.29	NS
No NP	0 Gy	12.7	5.4		
	2 Gy	25.2	1.4		
	4 Gy	38.4	1.9		
	6 Gy	45.8	3.8		

P values are generated from t-test results using different NP-treated groups in comparison with the non-NP-treated control group at the same dose of X-ray. $P<0.01$ was considered statistically significant.

Table S2. Statistical analysis for **Fig. S24.** of the Supplementary information. Student's two-tailed t-tests were performed in Excel with reference to the No NP, 0 Gy control.

		Viability (%)		Student's T test	
	X-ray dosage	**Average**	**s.d.**	***P***	**Significance**
SeNP	0 Gy	75.6	3.6	0.024	NS
	6 Gy	69.6	8.4	0.78	NS
No NP	0 Gy	68.2	0.9		
	6 Gy	53.5	1.6	0.00015	**

P values are generated from t-test results using SeNP groups in comparison with the non-NP-treated control group at the same dose of X-ray. $P<0.01$ was considered statistically significant.

Table S3. Statistical analysis for **Figure 4G** of the main text. Cell population percentage in G2/M phase after X-ray irradiation. Student's two-tailed t-tests were performed in Excel.

		G2/M population (%)		Student's T test	
	X-ray dosage	**Average**	**s.d.**	***P***	**Significance**
Selenomelanin ghost	0 Gy	11.8	3.5	0.53	NS
	2 Gy	14.8	3.1	0.00053	***
	4 Gy	22.9	1.9	2.3E-06	*****
	6 Gy	26.1	1.0	8.5E-06	*****
No NP	0 Gy	13.6	4.9		
	2 Gy	25.8	3.0		
	4 Gy	37.9	1.0		
	6 Gy	44.5	4.0		

P values are generated from the t-test results using selenomelanin ghost and non-treated groups at the same dose of X-ray. $P<0.01$ was considered statistically significant.

References

1. Pyo, J.; Ju, K. Y.; Lee, J. K., Artificial pheomelanin nanoparticles and their photo-sensitization properties. *J. Photochem. Photobiol. B* **2016,** 160, 330-5.

2. Liu, Y.; Kempf, V. R.; Brian Nofsinger, J.; Weinert, E. E.; Rudnicki, M.; Wakamatsu, K.; Ito, S.; Simon, J. D., Comparison of the Structural and Physical Properties of Human Hair Eumelanin Following Enzymatic or Acid/Base Extraction. *Pigment Cell Res.* **2003,** 16, (4), 355-365.

3. Abcam Flow cytometric analysis of cell cycle with propidium iodide DNA staining. https://www.abcam.com/protocols/flow-cytometric-analysis-of-cell-cycle-with-propidium-iodide-dna-staining

4. Ju, K. Y.; Lee, Y.; Lee, S.; Park, S. B.; Lee, J. K., Bioinspired Polymerization of Dopamine to Generate Melanin-Like Nanoparticles Having an Excellent Free-Radical-Scavenging Property. *Biomacromolecules* **2011,** 12, (3), 625-632.

5. Zhou, X.; McCallum, N. C.; Hu, Z.; Cao, W.; Gnanasekaran, K.; Feng, Y.; Stoddart, J. F.; Wang, Z.; Gianneschi, N. C., Artificial Allomelanin Nanoparticles. *ACS Nano* **2019,** 13, (10), 10980-10990.

6. Wang, Z.; Tschirhart, T.; Schultzhaus, Z.; Kelly, E. E.; Chen, A.; Oh, E.; Nag, O.; Glaser, E. R.; Kim, E.; Lloyd, P. F.; Charles, P. T.; Li, W.; Leary, D.; Compton, J.; Phillips, D. A.; Dhinojwala, A.; Payne, G. F.; Vora, G. J., Characterization and application of melanin produced by the fast-growing marine bacterium *Vibrio natriegens* through heterologous biosynthesis. *Appl Environ Microbiol* **2019**, DOI: 10.1128/AEM.02749-19.

7. Schweitzer, A. D.; Howell, R. C.; Jiang, Z.; Bryan, R. A.; Gerfen, G.; Chen, C.-C.; Mah, D.; Cahill, S.; Casadevall, A.; Dadachova, E., Physico-Chemical Evaluation of Rationally Designed Melanins as Novel Nature-Inspired Radioprotectors. *PLOS ONE* **2009,** 4, (9), e7229.

8. Mbonyiryivuze, A.; Mwakikunga, B.; Dhlamini, S. M.; Maaza, M., Fourier Transform Infrared Spectroscopy for Sepia Melanin. *Phys. Mater. Chem.* **2015,** 3, (2), 25-29.

9. Ito, S.; Wakamatsu, K., Chemistry of Mixed Melanogenesis—Pivotal Roles of Dopaquinone. *Photochem. Photobiol.* **2008,** 84, (3), 582-592.

10. Ito, S., Optimization of conditions for preparing synthetic pheomelanin. *Pigment Cell Res* **1989,** 2, (1), 53-6.

11. MacLeod, M. J.; Johnson, J. A., PEGylated N-Heterocyclic Carbene Anchors Designed To Stabilize Gold Nanoparticles in Biologically Relevant Media. *J. Am. Chem. Soc.* **2015,** 137, (25), 7974-7977.

12. Ito, S.; Novellino, E.; Chioccara, F.; Misuraca, G.; Prota, G., Co-polymerization of dopa and cysteinyldopa in melanogenesis *in vitro*. *Experientia* **1980,** 36, (7), 822-3.

13. Xiao, M.; Li, Y.; Allen, M. C.; Deheyn, D. D.; Yue, X.; Zhao, J.; Gianneschi, N. C.; Shawkey, M. D.; Dhinojwala, A., Bio-Inspired Structural Colors Produced *via* Self-Assembly of Synthetic Melanin Nanoparticles. *ACS Nano* **2015,** 9, (5), 5454-5460.

14. Kawamura, A.; Kohri, M.; Morimoto, G.; Nannichi, Y.; Taniguchi, T.; Kishikawa, K., Full-Color Biomimetic Photonic Materials with Iridescent and Non-Iridescent Structural Colors. *Sci Rep* **2016,** 6, 33984.

15. Huang, Y.; Li, Y.; Hu, Z.; Yue, X.; Proetto, M. T.; Jones, Y.; Gianneschi, N. C., Mimicking Melanosomes: Polydopamine Nanoparticles as Artificial Microparasols. *ACS Cent. Sci.* **2017,** 3, (6), 564-569.

16. Etebari, M.; Jafarian-Dehkordi, A.; Lame, V., Evaluation of protective effect of amifostine on dacarbazine induced genotoxicity. *Res Pharm Sci* **2015,** 10, (1), 68-74.